Recent climate change reduced Spanish forests' carbon sink capacity

Diego Bengochea Paz[1*], Ana Rey[1], Miguel Angel Zavala[2], Miguel B. Araújo[1,3,4]

[1] *Department of Biogeography and Global Change, National Museum of Natural Sciences, Consejo Superior de Investigaciones Científicas (CSIC), Calle Jose Gutierrez Abascal, 2, 28006 Madrid, Spain*

[2] *Departamento de Ciencias de la Vida, Grupo de Ecología y Restauración Forestal (FORECO), Universidad de Alcalá, Madrid, Spain*

[3] *Rui Nabeiro Biodiversity Chair, MED – Mediterranean Institute for Agriculture, Environment and Development & CHANGE – Global Change and Sustainability Institute, Universidade de Évora, Largo dos Colegiais, 7004-516 Évora, Portugal*

[4] *German Centre for Integrative Biodiversity Research (iDiv), Halle-Jena-Leipzig, Puschstrasse 4, Leipzig 04103, Germany*

[*] *Corresponding author: diego.bengochea@mncn.csic.es*

https://orcid.org/0000-0002-0835-3981

November the 13th, 2025

Peer-review statement: This manuscript is a non-peer reviewed preprint submitted to EarthArXiv. The manuscript is currently under peer-review at Ecological Applications.

Abstract

Forests play a crucial role as carbon sinks and are central to climate mitigation strategies, yet their long-term reliability in this function is increasingly uncertain under climate change. Using deep learning techniques on a multi-source dataset—combining multi-spectral satellite data, airborne laser scanning, and ground-based measurements—we produced the most up-to-date high-resolution maps of woody carbon storage in continental Spain on a yearly basis from 2017 to 2024. Our analysis revealed substantial forest carbon losses, with Spanish forests and woodlands functioning as a net carbon source during this period, losing approximately 12% of their biomass carbon stocks, with the sharpest decline occurring during 2022 following the most intense drought of the century. *Eucalyptus* plantations and conifer forests experienced the greatest relative losses, 30% and 22% respectively, while low-density woodlands and agroforestry systems showed the greater resilience, with woody carbon stocks dropping only 5% in these areas. Our results support structural overshoot, where periods of favorable growing conditions promote vegetation growth that subsequently becomes vulnerable during drier conditions. Specifically, large rainfall and cooler summer temperatures were strongly correlated with subsequent time-lagged carbon losses. These findings reveal a critical challenge for climate policy as forest mitigation potential is hampered by climate change impacts, especially in Mediterranean regions where drought intensity is increasing. This highlights the urgent need to align adaptation and mitigation policies to enhance forest resilience and its long-term climate mitigation capacity.

Keywords: artificial intelligence; biomass dynamics; carbon sink; climate change; climate change mitigation; ecological modelling; forest carbon; neural networks; remote sensing; structural overshoot;

1 Introduction

Forest ecosystems play an important role in regulating the Earth's climate by absorbing atmospheric carbon dioxide (CO_2) and storing carbon in forest biomass, making them central to nature-based climate mitigation strategies (Shanley et al. 2024). In addition, forests influence land surface temperature, albedo, and evapotranspiration, contributing to local climate regulation and climate adaptation efforts (Alibakhshi et al. 2024). Forests also provide a suite of essential ecosystem services, including biodiversity support, water regulation, soil stabilization, and recreational and cultural benefits (Felipe-Lucia et al. 2018).

Increasing concentrations of atmospheric CO_2 boosted vegetation productivity during the 20th century, strengthening forests' carbon sequestration capacity. However, recent research warns of a weakening of this effect, with some studies anticipating a shift toward net CO_2 emissions(Peñuelas et al. 2017; Wang et al. 2020; Guo et al. 2025), particularly in warming regions of southern and northern Europe (Forzieri et al. 2021). Forest biomass gains observed in the late 20th and early 21st centuries have reversed since 2010 (Nabuurs et al. 2013) largely due to climate-induced dieback and increasing disturbance regimes observed worldwide (Peñuelas et al. 2017; Patacca et al. 2023). Alarmingly, tree mortality rates have doubled since the late 1900's, now affecting approximately 1% of Europe's forested area annually (Patacca et al. 2023). Accurate and timely estimation of forest carbon storage trajectories is critical to effectively manage forests for climate change mitigation and adaptation.

Recent technological advances have created renewed opportunities for forest carbon storage estimation and monitoring. State-of-the-art, high-resolution, forest biomass models integrate multi-source datasets—combining ground measurements from forest inventories, LiDAR-derived forest height estimations, and multispectral satellite imagery (Schwartz et al. 2023; Tanase et al. 2024). A key breakthrough involves using convolutional neural networks (CNNs) to infer LiDAR-derived canopy height from satellite data (Lang, Schindler, et al. 2019), addressing spatial and temporal limitations of geospatial LiDAR (Duncanson et al. 2022). This advance enables the production of continuous, high-resolution canopy height

maps, from which biomass and carbon stocks can be estimated using allometric models tailored to specific forest types.

Despite these methodological advances, few studies have focused on reconstructing forest biomass time series (e.g. Tanase et al. 2024; Su et al. 2025), and knowledge gaps remain in understanding how climate anomalies drive forest carbon storage dynamics and on the ecological and management factors that shape forest resilience. This study addresses this gap by applying advanced deep learning techniques to multi-source forest data to assess forest carbon changes across Spain during 2017-2024. Specifically, we estimate spatial and temporal patterns of above and belowground biomass carbon losses and gains, identify the most affected forest types and regions, and analyse the role of climate anomalies in driving these dynamics using state-of-the-art artificial intelligence techniques.

Iberian diverse forests—including Mediterranean, Atlantic, and montane ecosystems—make it an ideal case study for exploring broader European forest vulnerabilities to climate change. The forests in the Iberian Peninsula are particularly vulnerable to climate change, notably rising temperatures and prolonged and more intense droughts, increased extreme weather events, which are all projected to intensify in coming decades (Carnicer, Coll, et al. 2011; Dasari et al. 2014; Vicente-Serrano et al. 2014; Lazoglou et al. 2024). Projected climate trajectories are likely to exceed the tolerance thresholds of many tree species (García-Valdés, Zavala, et al. 2013; García-Valdés, Svenning, et al. 2015; Wessely et al. 2024), potentially compromising their growth rates and carbon storage capacity (Chiti, Rey et al. 2024).

Our analyses reveal concerning trends that challenge the prevailing assumption of Spanish forests as stable carbon sinks. Significant carbon losses across Spanish forests were recorded during the study period, revealing a shift from forests acting mainly as carbon sinks to becoming a source. We also identify critical climate-carbon relationships, supporting a 'structural overshoot' effect where multiple-year periods of higher precipitation and favorable temperatures stimulate growth that subsequently becomes vulnerable during drier and hotter conditions, potentially exacerbating forest dieback, wildfire risk and therefore carbon emissions. Notably, we observed that woodlands and agroforestry systems had more

stable carbon stocks compared to forest ecosystems, suggesting structural and compositional factors that enhance resilience to climate pressures. These findings demonstrate increasing vulnerability of forest carbon stocks to climate change, highlighting the importance of strategic forest management to maintain carbon sequestration capacity in Mediterranean regions facing intensified aridity and temperature extremes.

2 Methods

2.1 Overview

We developed a model of forest carbon storage integrating biomass estimations from national forest inventories, canopy height measurements from airborne laser scanning (ALS), and multi-spectral imagery from the Sentinel-2 satellite mission. Our modeling pipeline consists of three main steps: (1) inferring forest canopy height from multi-spectral satellite data, (2) calibrating allometric relationships between canopy height and forest biomass, and (3) mapping biomass stocks from forest height maps (Figure 1). We derived carbon stocks from biomass values using a fixed conversion factor of 0.5. This approach overcomes the spatiotemporal limitations of forest inventory biomass data and the temporal constraints of ALS height measurements, enabling us to produce high-resolution biomass density estimates with annual frequency across the entire country.

In the following sections, we describe the data sources used in our study, explain how we integrated multi-source data within our three-step deep learning modeling framework, and detail our model validation strategy. Finally, we present the statistical approach that we used to analyse the relationship between climate anomalies and changes in carbon storage.

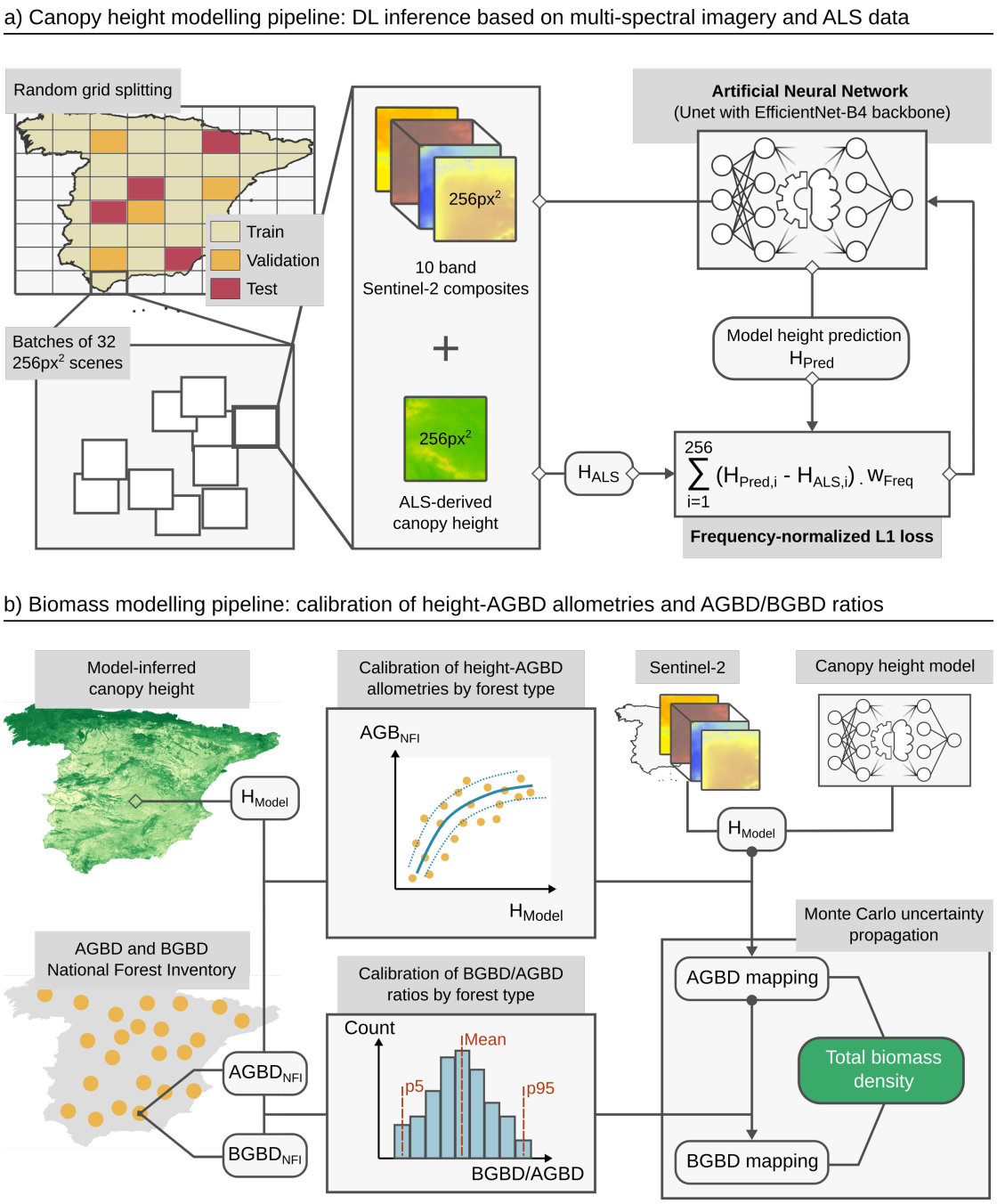

Figure 1: Graphical representation of the modelling pipeline. a) Deep learning pipeline for canopy height estimation. The dataset territory is divided into 64 tiles (80% training, 10% validation, 10% testing). Within each tile, 32 scenes of 256 px^2 are sampled to maximize height diversity. Each scene contains 10 Sentinel-2 bands and ALS-estimated canopy height. A CNN processes Sentinel-2 data to predict height, with backpropagation minimizing a frequency-normalized absolute loss function. b) Biomass estimation from canopy height maps. Modeled height data are combined with NFI4 AGBD measurements to calibrate height-AGBD power-law allometries. AGBD and BGBD data establish root-to-shoot ratios. The integrated pipeline processes Sentinel-2 imagery through the trained CNN for height inference, converts height to AGBD using calibrated allometries, and calculates BGBD using established ratios. Monte Carlo simulation estimates uncertainty by sampling AGBD and BGBD values from quantile regression allometries and ratio distributions.

2.2 Biomass data source: national forest inventory data

We utilized data from the fourth Spanish national forest inventory (NFI4) (Ministerio para la Transición Ecológica y el Reto Demográfico 2025a), which began in 2008 and remains ongoing. The NFI4 reports biomass stocks stratified by species and diameter class. For each 5 m radius experimental plot, we calculated total aboveground and belowground biomass density (AGBD and BGBD, respectively) by summing contributions across all species and diameter classes (reported in the NFI4 data table 'Parcelas_exs', under fields 'BA' for AGBD and 'BR' for BGBD). In provinces that reported growing stock volume instead of biomass stocks, we applied species or taxon-specific wood density estimates (Chave et al. 2009)to convert volume to biomass. We referenced each biomass measurement to its corresponding plot sampling year. This processing yielded a comprehensive spatio-temporal dataset of AGBD and BGBD, enriched with forest type classifications according to the official national categorization published in the most updated official Spanish forestry map (MFE 25) (Ministerio para la Transición Ecológica y el Reto Demográfico 2025b) following the 'Tree Formation' ('Formación Arbolada') data field.

2.3 Forest type data source: Spanish forest map (MFE25)

Forest type classification was based on MFE 25. This classification system categorizes woody ecosystems according to dominant tree formations. Areas with homogeneous composition ($\geq$ 70% single species) were classified by species or genera, while heterogeneous formations were designated as mixed forests and further subdivided by ecoregion (Alpine, Atlantic, or Mediterranean). The classification also includes a 'tree-less' ('No arbolado') category comprising agroforestry systems (including orchards and olive groves), urban forests and low-density or low-height woodlands, which together constitute 62% of Spanish territory (Table S1). Despite their 'tree-less' classification in official statistics, these land areas contain woody biomass and were therefore included in our carbon storage assessment.

2.4 Canopy height data source: airborne laser scanning

We employed normalized vegetation height maps developed by the Spanish National Geographic Institute (Instituto Geográfico Nacional 2021). These maps derive from ALS data collected under the Spanish national plan of aerial orthophotography (PNOA LiDAR, Instituto Geográfico Nacional 2021) and provide vegetation height measurements at 2.5-meter resolution across the entire country. The height maps were generated by normalizing LiDAR height measurements against terrain height according to slope and by masking artificial surfaces to isolate vegetation. Our analysis incorporated data from the second (2015-2021) PNOA LiDAR mission. Note that national coverage is obtained by compositing measurements from different years, which implies that different regions were sensed at different times.

2.5 Multi-spectral data source: Sentinel-2 imagery

We computed composite images of Sentinel-2 Level-2A observations from 2017 to 2024, accessed via the Earth Search STAC API (Copernicus Sentinel data 2024). We produced the median composites using images gathered between June the first and September the first. We carried over the selection of scenes by filtering out images with high cloud cover in an iterative process. Starting by imposing a cloud threshold of 90% and decreasing by steps of 10% we selected at least 40 scenes. Then, we selected the best 12 according to quality criteria regarding the presence of no-data and clouds in the images. We used 12 scenes as a compromise between stability in the composite estimation and robustness of the median calculation. As a result we obtained cloud-free mosaics of 10 Sentinel-2 bands at a resolution of 10 meters for the 2017 to 2024 range (bands 2, 3, 4, 5, 6, 7, 8, 8A, 11 and 12). We excluded the three bands at 60 meters resolution designed to identify clouds and aerosol thickness (bands 1, 9 and 10). All bands at 20 meters resolution were upsampled to 10 meters using bilinear interpolation (bands 5, 6, 7, 8A, 11 and 12).

2.6 Canopy height inference from Sentinel-2 imagery

We adopted a deep learning approach and trained a convolutional neural network (CNN) to infer ALS-derived canopy height from 10-band Sentinel-2 imagery (Lang, Jetz, et al. 2023). CNNs offer important advantages over classical machine learning models such as random forests for spatially-structured regression tasks like forest canopy height estimation (Ball et al. 2017; Shah et al. 2020). Unlike pixel-by-pixel mapping methods, CNNs process information from the entire scene to make pixel-level predictions, enabling them to better capture spatial patterns and texture—a crucial capability for high-resolution mapping (Ball et al. 2017).

We constructed our training dataset by pairing Sentinel-2 imagery with corresponding ALS-derived canopy height data from matching sampling years. This yielded a composite dataset spanning 2017 to 2021, which we processed simultaneously for model training. To ensure spatial alignment between data sources, we downsampled the high-resolution canopy height images to 10-meter resolution using averaging techniques, matching the native resolution of Sentinel-2 data. The resulting training dataset encompasses 160,292 km^2 and captures the Spanish latitudinal gradient, spanning Mediterranean and Eurosiberian biogeographical regions (Appendix S1: Figure S1a; Loidi and Vynokurov 2024).

We divided the dataset into training, validation, and testing subsets following an 80%, 10%, and 10% distribution, respectively. The splitting procedure employed a random grid assignment with a grid size of 8, effectively subdividing the Spanish territory into 64 square tiles with a side-length of approximately 120 km. Data was allocated to each subset by sampling uniformly across these tiles while ensuring that all data within the same tile remained in the same subset. This approach mitigates the influence of spatial autocorrelation on performance metrics, thereby promoting model generalization and providing a more realistic assessment of prediction accuracy (e.g., Araújo, Pearson, et al. 2005).

Predicting canopy height with CNNs faces a significant challenge due to the skewed distribution of forest heights toward lower values (Lang, Jetz, et al. 2023). This challenge is

particularly pronounced in Spain, which encompasses two markedly distinct biogeographical regions: Mediterranean and Eurosiberian (Loidi and Vynokurov 2024). Mediterranean forests, generally characterized by lower canopy heights, greatly outnumber Eurosiberian forests. Additionally, large regions exhibit homogeneous distributions of low and very low canopy heights. Consequently, CNN models tend to over-specialize in lower height ranges, severely underestimating taller forest patches.

To address this challenge, we implemented two strategic approaches. First, we selectively undersampled the original dataset by eliminating ALS-derived height tiles based on specific criteria: tiles containing more than 50% artificial surfaces or those with a 90th percentile height below 15 meters were excluded. Second, we developed a custom batch sampler to prioritize training scenes with greater height diversity, thereby exposing the CNN to more varied data and enabling it to learn complex height distributions.

Our sampling algorithm employed a two-stage filtering process to generate 32 training patches of 256px^2 each. Initially, the algorithm verified scene acceptability by selecting only those containing more than 40% vegetated surfaces with heights above one meter. Once a scene passed these basic criteria, the algorithm calculated a diversity score—the geometric mean of the scene's height distribution standard deviation, height range, and interquartile range. Scenes were accepted if their diversity score exceeded a threshold value. To ensure efficient convergence, we implemented a progressive relaxation mechanism for the diversity threshold as sampling attempts increased, ultimately accepting any qualifying scene after 1200 attempts. This approach created balanced training batches representing the full spectrum of forest height distributions while preventing oversampling of low-height Mediterranean forests.

We employed a Unet architecture (Ronneberger et al. 2015) CNN with an Efficient Net-B4 (Tan and Le 2019) encoder backbone, comprising 20.2 million parameters. Originally developed for medical imagery, the Unet architecture excels at identifying multi-scale features in images and has been successfully applied to forest structure modeling in France and the Iberian peninsula (Schwartz et al. 2023; Su et al. 2025). This architecture offers important

advantages for our application: it is relatively lightweight, requires shorter training times than comparable alternatives, and delivers state-of-the-art performance even when initialized with random weights and without incorporating a priori knowledge.

Following Lang, Jetz, et al. (2023), we implemented a batch-balanced L1-loss function to further mitigate the skewness in height distribution that persisted despite our undersampling and diversity sampling strategies. We calculated batch sample frequencies in one-meter width bins and weighted the L1-loss contribution of each pixel by the square root of the inverse sample frequency. The square root exponent was selected after empirical testing confirmed it provided optimal balance across height ranges. As Lang, Jetz, et al. (2023) observed, linear scaling tends to overcompensate and substantially reduces performance in lower height ranges. Although this resulted in an increase of overall Mean Absolute Error, the approach prevents the numerically dominant lower height ranges from controlling loss calculation, resulting in more consistent performance across the entire height spectrum.

We trained the model for 100 epochs using a One Cycle learning rate scheduler with cosine annealing (Smith and Topin 2017). This training schedule dynamically adjusts the learning rate throughout training, beginning with an increasing "warm-up" phase followed by a cosine-function decrease until training completion. The One Cycle approach accelerates model convergence by facilitating broader exploration of the loss landscape during warm-up, then progressively fine-tuning toward an optimal final model during the decay phase. We configured the scheduler with a peak learning rate of 2e-4 and applied downscaling factors of 15 and 100 for the start and end, respectively, with the peak occurring at 20% of total training progress.

We monitored training progress by analyzing the distribution of mean absolute errors (MAE) across multiple height bins on the validation dataset. From the five models with the lowest validation loss, we selected the one exhibiting the most balanced error distribution across all height ranges. When evaluated on the test dataset, our selected model achieved an overall MAE of 3.40 meters with a bias of 2.31 meters. The model performed well in the 0 to 20 meter range, with optimal performance between 6 and 15 meters, though it

showed substantial underestimation for heights exceeding 25 meters. However, the practical impact of this underestimation is mitigated by the height distribution in the ALS-derived reference data, where 95% of pixels have heights below 12 meters (Appendix S1: Figure S2). Consequently, our model demonstrates robust performance across the height ranges that dominate Spanish forest landscapes. We applied this optimized model to generate annual canopy height maps for the entire Spanish territory at 10-meter resolution for 2017-2024.

2.7 Calibration of height-biomass allometric relationships

We calibrated height-biomass allometric relationships stratified by forest type, following the classification of the MFE25. To limit error propagation from the canopy height model to biomass estimations, we calibrated allometries using model-predicted heights rather than ALS-derived heights. Biomass data–both AGBD and BGBD–were obtained from the processing of the NFI4, as explained previously. To ensure the obtention of total biomass values, we calibrated forest type-level BGBD to AGBD ratios. The total calculation was, therefore, carried out in two steps: first inferring AGBD from canopy height, and then BGBD by applying the calibrated ratio. Both datasets span Spain's latitudinal gradient, though the height-AGBD dataset exhibits an overrepresentation of Mediterranean forest types relative to Eurosiberian (Appendix S1: Figure S1b,c).

We used power-law functions for the height-AGBD allometries and only calibrated allometries for forest types with more than 10 samples. To address the limitation that multiple forest types lacked sufficient samples, we developed a hierarchical database of allometries divided into five tiers (Table S2). The first tier groups all samples together, corresponding to a general allometry. The second tier separates forest types by plant clade into angiosperm-dominated, gymnosperm-dominated, and mixed forests. The third tier separates forest types by taxonomic family of the dominant species; in forests with mixed species of the same clade, this tier preserves clade information, while in the absence of more specific information or for species and clade-mixed forests, it maintains the second-tier label. The fourth tier distinguishes forests by genus of the dominant species; for mixed forests, this tier contains

information on biogeographical regions. Finally, the fifth tier separates non-mixed forest types by dominant species.

For each group within each tier with enough samples, we performed linear regressions in the logarithmic space for power-law fits. Additionally, we performed quantile regressions for the 15th and 85th percentiles, allowing us to obtain uncertainty estimates of the height-AGBD relationships (Table S2). We based our choice for 15th and 85th percentiles–instead of the more standard 2.5th and 97.5th percentiles–because of limitations with the dataset's size. Using more extreme percentiles leads to the fits in quantile regression to be dominated by a low number of points that could include outliers leading to artificially broad confidence intervals.

We calibrated BGBD over AGBD ratios by forest type exclusively using the Spanish NFI data. For each forest type, we calculated the average ratio, as well as the 5th and 95th percentiles, enabling us to estimate uncertainty bands (Table S3). We followed the same hierarchical classification of forest types as for the height-AGBD relationships, and discarded all forest types with less than 25 samples. We identified outliers prior to the calculation using the interquartile range method and values beyond 1.5 times the interquartile range from quartiles were excluded. We assessed normality of BGBD over AGBD ratio distributions using skewness and kurtosis criteria following established statistical guidelines (George and Mallery 2019). Distributions were classified as normal when absolute skewness values were ≤ 2 and absolute kurtosis values were ≥ 7 (George and Mallery 2019). All ratio distributions, for all forest types across tiers amply satisfied normality criteria (Table S4).

2.8 Biomass mapping: expected values and uncertainty range

We used the calibrated height-AGBD allometries and BGBD over AGBD ratios to process the model-derived canopy height maps and estimate expected biomass and uncertainties in each pixel. We employed a Monte Carlo sampling approach to generate populations of 1,000 biomass values per pixel by utilizing the percentile information from the allometries and

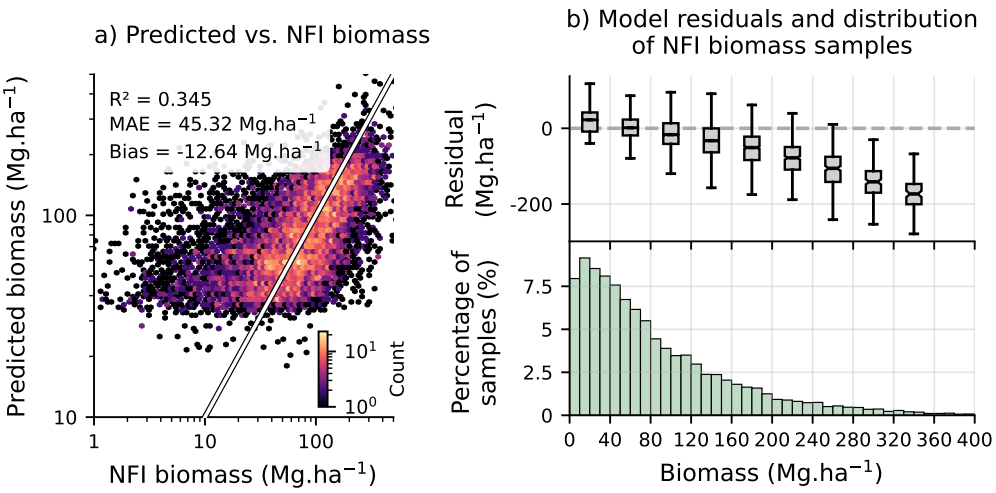

Figure 2: Biomass model evaluation. (a) 2-D histogram of model-predicted biomass (y-axis) against NFI4-reported biomass (x-axis). Axes are in logarithmic scale to facilitate visualization. Colors depict the frequency of occurrence of each pixel, where pixels close to the 1:1 line (solid white line with black edges) are perfect predictions, and pixels on the left and right of the 1:1 line correspond to overestimations and underestimations, respectively. Regression metrics are reported on the top left of the panel, where R^2 is the regression's coefficient of determination and MAE the mean absolute error. (b) Representation of model residuals across biomass bins (top) and distribution of biomass values in NFI4 samples (bottom).

ratios. For the height-AGBD allometries, we assumed that at every height, the distributions of AGBD values followed a normal distribution, with means estimated via linear regression. The regressions for 15th and 85th percentiles were used to estimate the distribution's standard deviation using corresponding z-scores. We adopted the same approach for the BGBD over AGBD ratios, reconstituting a normal distribution for each forest type based on reported mean and the 5th and 95th percentiles of the ratio distributions. While the assumption of normality is difficult to validate empirically—particularly given potential asymmetries in the underlying data—it provides a computationally efficient framework for uncertainty propagation within the Monte Carlo simulations. Alternatives such as non-parametric resampling or percentile-based interval estimation could better capture non-Gaussian features but are considerably more demanding computationally and would limit the number of replicas, thus reducing the robustness of the uncertainty estimates. The normal approximation, despite symmetrising potentially asymmetric uncertainties, enables a large number of Monte Carlo iterations and more stable inference.

In each pixel, we generated 1,000 random AGBD samples according to the normal distribution associated with the pixel height. Similarly, we generated 1,000 BGBD over AGBD ratios from the corresponding distribution, enabling us to calculate BGBD for each sample. We then estimated the total biomass by summing the AGBD and BGBD values and calculated the mean and standard deviation across all samples in each pixel. The mean value represents the expected biomass, while we derived 95% confidence intervals from the samples' standard deviation to quantify uncertainty. Through the application of these procedures, we produced yearly maps of expected AGBD, BGBD, and total biomass, along with their respective uncertainties, for 2017-2024. Uncertainty bands at the national level (see Figure 3c) were calculated assuming a spatially autocorrelated error at a distance of 80 km. This distance matches the spatial extent of the Sentinel-2 mosaics that we produced for model training, ensuring that we provide realistic uncertainty margins in accordance with our data processing pipeline.

Annual crops (irrigated and non-irrigated) and rice fields were excluded from the analysis using the CORINE land cover dataset 2018 (Copernicus Land Monitoring Service 2020). These land cover types were masked due to their spectral similarity to tall forests, which would otherwise introduce significant estimation biases in woody biomass carbon quantification.

We validated our biomass estimation by comparing our predictions of expected biomass with the measurements of the NFI4 and obtained a MAE of 45 $Mg.ha^{-1}$, a bias of -13 $Mg.ha^{-1}$ and a R^2 of 0.35 (Figure 2a). An analysis by biomass ranges shows that large underestimations are mostly concentrated in experimental plots with larger biomass values, which are also the rarest plots (Figure 2b). The model shows best performance in the most common biomass ranges (0-160 $Mg.ha^{-1}$).

2.9 Relationship between climatic anomalies and carbon storage dynamics

We examined the relationship between climatic anomalies (relative to a 1984-2014 baseline) and interannual vegetation carbon storage changes during 2017-2024. Our analysis aimed to: (1) characterize the predictive power of climatic anomalies on interannual carbon changes; and (2) identify the most influential climatic variables driving this relationship.

Monthly precipitation and 2-meter temperature data (10km resolution) from the ERA5-Land dataset (Muñoz Sabater 2019) were processed to establish baselines for standard WorldClim bioclimatic variables (Table S4). We excluded temperature diurnal range (BIO2) and isothermality (BIO3), which require daily data, and four interactive variables (BIO8, BIO9, BIO18, BIO19) that combine precipitation and temperature to minimize spatial artifacts (Booth 2022). To align with our summer-based carbon estimations, we calculated bioclimatic variables using rolling years (September to August) and derived anomalies as deviations from the baseline. We computed both same-year anomalies and accumulated anomalies over two and three years for both precipitation and temperature-related variables, yielding 39 variables total (Table S4).

Carbon density maps were downsampled to match climate data resolution by averaging, and relative interannual changes were calculated using a symmetric measure. We selected relative over absolute changes because carbon response magnitude is typically proportional to existing stocks. The symmetric approach produced bounded values and prevented computational issues in areas with close to 0 carbon storage undergoing regrowth. We compiled a tabular dataset of relative carbon changes and standardized climate anomalies for all pixels and years. To address spatial autocorrelation and enhance model generalizability, we partitioned the dataset into 15 spatial blocks using K-means clustering (15 clusters). This approach yielded an average cluster radius of 180 kilometers, largely exceeding the autocorrelation distance of relative carbon changes ($\tilde{5}0$ km on average, Appendix S1: Figure S3), which ensures statistical independence between training and test sets.

We conducted a predictor selection experiment using 4,000 independent Bayesian optimizations to identify predictor sets that maximized goodness-of-fit (R^2) in held-out test data. Each optimization trained on eight randomly selected spatial blocks and validated on three others. The top 10% performing models were evaluated on an additional held-out test set of three randomly selected spatial blocks, with only the best-performing model retained per run. We employed a Tree-structured Parzen Estimator method (300 trials per run) with early stopping (after 100 minimum trials and 40 trials without improvement). To maintain parsimony and computational efficiency, we limited each model to a maximum of 10 features from the 39 potential predictors.

We evaluated the feature selection experiment by examining selection frequency, importance, and redundancy across models. Feature importance was quantified using Shapley values—a game-theoretical metric that measures the magnitude and direction of each feature's contribution to model outputs (Lipovetsky and Conklin 2001; Štrumbelj and Kononenko 2014)—implemented through the SHAP Python package (Lundberg 2017). Feature redundancy was assessed via permutation importance (Breiman 2001), which measures outcome changes when predictor values are shuffled, using scikit-learn (Pedregosa et al. 2011). Smaller values indicate redundancy, suggesting alternative features convey similar information. We further analyzed the direction and magnitude of feature effects by examining the response of Shapley values to changes in features' values across all optimal models. We used a LOWESS smoothing of the data from all optimal models as a proxy for the average effect of each feature across models. This feature-by-feature analysis allows us to estimate how the variations in climatic anomalies affect interannual carbon changes. This is presented in Figure 5a and the full dependency curves for all models together with the LOWESS-smoothed curve are shown in Appendix S1: Figure S9.

3 Results

3.1 Changes in forest carbon storage from 2017 to 2024

Forest carbon stocks declined across most Spanish carbon hotspots between 2017 and 2024, with notable exceptions in the central Pyrenees, along the Cantabrian mountain range, and in eastern Galicia (Figure 3a & 3b). At the country level, forest carbon storage decreased by 11.7% over the study period, primarily as a result of a sharp 12.9% drop between the summers of 2021 and 2022 (Figure 3c, Appendix S1: Figure S5). We estimated a decrease in carbon storage in four out of seven interannual transitions, resulting in a cumulative loss of 150 MtC over the full study period (Figure 3d).

Conifer forests experienced the most substantial carbon losses, declining by 65 MtC (21%) (Figure 4a). *Pinus* spp. forests dominate these losses, though all conifer species showed marked declines (Figure 4b). Broadleaved forests display the widest range of carbon responses—*Eucalyptus* spp. plantations decreased by 30% while *Fagus* spp. increased by 6% (Figure 4a). Overall, broadleaved forests lost 43 MtC between 2017-2024, and *Quercus* spp. forests, the dominant broadleaved carbon reservoir, declined by 8%. Mixed forests declined across all biogeographical regions (Alpine, Atlantic, and Mediterranean), averaging a 20% carbon loss (Figure 4a). Low-density woodlands and agroforestry systems showed the smallest percentage losses (5%) while contributing 42% of Spain's total carbon storage in 2017 (Figure 4b)—a substantial contribution that reflects their extensive coverage of Spanish land (Table S1).

The distribution of biomass carbon stocks by forest height shifted considerably over the study period. The proportion of carbon stored in shorter forests (2-6 meters) increased from 60% in 2017 to 70% in 2024, while taller forests (>10 meters) stored progressively less carbon (Figure 4c). This transformation primarily occurred during the 2021-2022 transition period.

The three dominant genera in Spain's carbon inventory—*Quercus* spp., *Pinus* spp., and *Eucalyptus* spp.—maintained stable carbon stocks until 2021 before experiencing abrupt

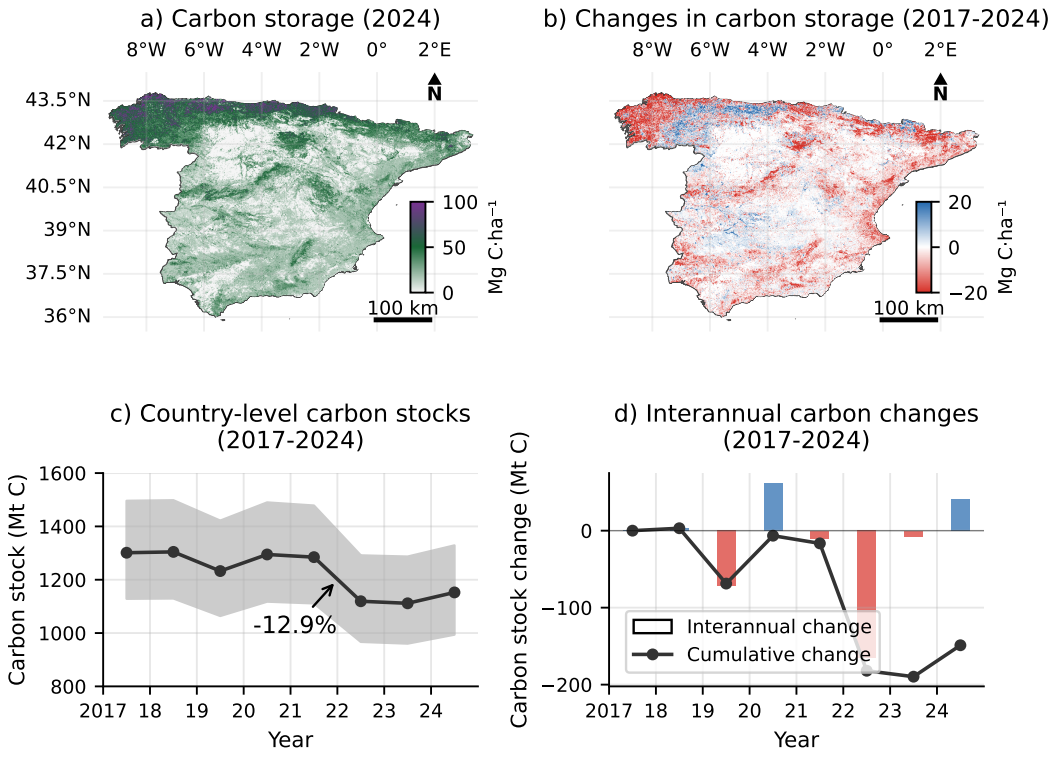

Figure 3: Changes in carbon storage in Spain (2017-2024). a) Map of vegetation carbon storage in Spain for 2024. The map excludes agricultural land cultivated with annual crops. The uncertainty map depicting 95% confidence intervals is shown in Appendix S1: Figure S4. b) Map of changes in carbon storage between 2017 and 2024 showing gains and losses in blue and red respectively. c) Temporal trend of total vegetation carbon stocks from 2017 to 2024. The black solid line shows the expected carbon stock and grey bands correspond to the 95% confidence interval of the estimation. d) Interannual carbon changes from 2017 to 2024. Red and blue bars correspond to negative and positive changes in vegetation carbon storage, respectively. The solid black line shows the cumulative change starting from 2017.

declines in 2022 coinciding with a very dry year (the driest in the century), followed by modest recoveries, particularly in *Quercus* spp. forests (Figure 4d). Among major carbon-contributing genera, only *Fagus* spp. showed slight overall gains throughout the study period, though with notable year-to-year fluctuations (Figure 4d).

3.2 Bioclimatic predictors of forest carbon changes

Bioclimatic anomalies relative to the 1984-2014 baseline emerged as moderate predictors of interannual carbon storage dynamics during 2017-2024. Across 4,000 independent feature selection experiments, our spatially cross-validated XGBoost models achieved a median R^2 of 0.28 (10th–90th percentile range: 0.12–0.39; Appendix S1: Figure S6).

The six most frequently selected bioclimatic predictors, each present in at least 30% of models with $R^2 > 0.2$, exhibit both high importance and low redundancy, quantified through Shapley values and a permutation importance metric, respectively (Figures S7 and S8). These six variables represent three key bioclimatic factors, each appearing in both same-year and multi-year accumulated versions: precipitation anomaly (same-year: selected in 46% of successful models; three-year accumulated: 43%), temperature anomaly (same-year: 31%; two-year average: 42%), and temperature seasonality anomaly (same-year: 31%; three-year average: 38%) (Figure 5a, Appendix S1: Figure S7 and S9).

In the absence of climate anomalies, models predict stable carbon storage, with effects intensifying as anomalies increase in magnitude (Figure 5a). Precipitation and temperature variables revealed contrasting effects depending on their temporal window. Negative current-year precipitation anomalies correlated with biomass carbon losses, yet negative accumulated precipitation anomalies correlated with carbon gains (Figure 5a). Temperature showed the inverse relationship: positive current-year anomalies correlated with losses, while positive accumulated temperature anomalies correlated with carbon gains (Figure 5a). Temperature seasonality exhibited strong single-year effects, with high positive anomalies correlated with carbon losses, whereas its three-year accumulated version showed weaker, non-monotonic

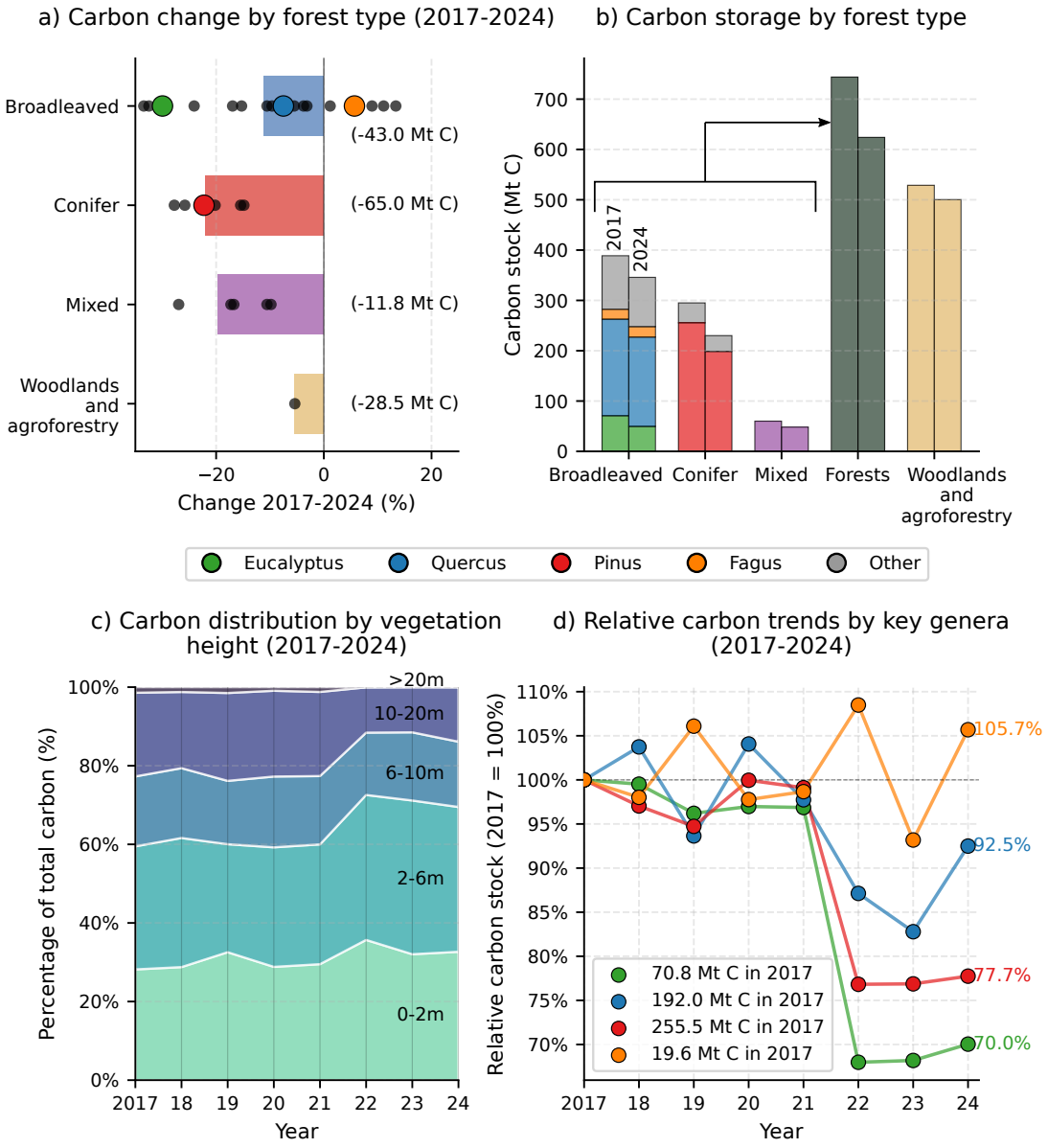

Figure 4: Differential changes in vegetation carbon storage across forest types. a) Percentage changes in carbon storage over 2017 to 2024 for different forest types. Black points correspond to forests dominated by different genera in conifer and broadleaved types and to different biogeographical regions in the mixed case. Colored points mark genera with meaningful contributions to total carbon storage in Spain. b) Carbon storage by forest type and key genera for 2017 and 2024. c) Evolution of the distribution of carbon storage across forest height ranges over 2017-2024. d) Evolution of carbon storage by key genera relative to stocks in 2017.

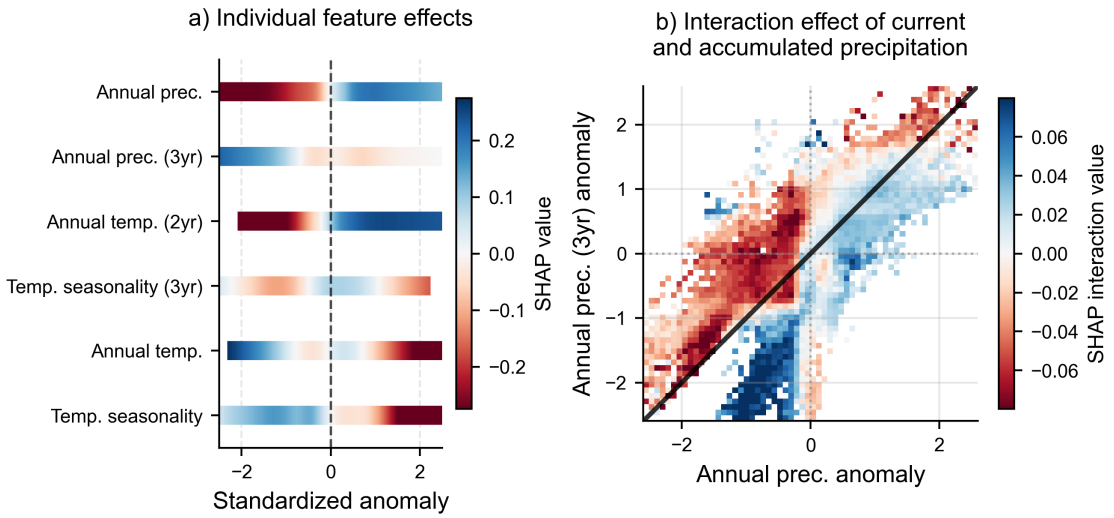

Figure 5: Correlations between climate anomalies and changes in vegetation carbon storage. a) Individual feature effects on interannual carbon changes averaged across 4,000 optimal models. Features are displayed in the y-axis and ordered by selection frequency (decreasing from top to bottom). We only show features selected in at least 30% of the optimal models with R_2>0.2. The x-axis shows the standardized anomalies for each of the bioclimatic variables. Color depicts the direction and strength of the average effect of different features across ranges. Red and blue colors indicate interannual carbon losses and gains respectively. b) Interaction effect of current-year and three-year accumulated precipitation on interannual carbon changes measured by Shapley interaction values, where negative and positive values indicate carbon losses and gains, respectively. The 1:1 line is shown in solid black.

effects (Figure 5a).

The analysis of the interaction effect of same-year and three-year accumulated precipitation revealed that positive anomalies in accumulated precipitation correlated with biomass carbon losses when same-year precipitation anomalies were negative (Figure 5b). This reflects a broader pattern where biomass carbon losses predominantly occur when accumulated precipitation anomalies exceed same-year anomalies, with the 1:1 line in Figure 5b serving as a boundary between regions of carbon loss and gain.

4 Discussion

The European Union strongly relies on forests to reduce CO_2 emissions by 55% in 2030 and to become carbon neutral by 2050, as part of the *European Green Deal* (Directorate-General for Communication (European Commission) 2021). However, climate change increasingly threatens the carbon sink capacity of forests, undermining their potential as nature-based climate solutions (Woude et al. 2023; Chen et al. 2024; Pan et al. 2024). Using state-of-the-art deep learning techniques to create the first forest carbon time-series extending to 2024 for continental Spain, we provide the most comprehensive assessment of both above and belowground biomass carbon dynamics at the national scale. Our study revealed that Iberian Spanish forests reduced their carbon sink capacity by losing 12% of their carbon stocks, and showed a clear relationship between biomass carbon losses and recent climate change. This raises serious questions about the effectiveness of unmanaged forests and woodlands as nature-based solutions to achieve climate neutrality by 2050.

4.1 Structural overshoot: when favorable climate increases vulnerability

Our analysis revealed that high average temperatures and more intense heat waves and droughts are strong predictors of woody biomass carbon losses from one year to the next. Instead, large precipitation is correlated with stock gains. Interestingly, we find that same-year and multi-year accumulated anomalies have opposing effects on woody biomass carbon stocks: large accumulated precipitation has negative to null effects on stocks, while large accumulated temperatures have a positive effect. We interpret this apparent paradox as evidence for structural overshoot dynamics where periods of favorable climate conditions embedded within broader unfavourable trends increase the vulnerability of woody carbon stocks (Yao Zhang et al. 2021).

Structural overshoot occurs when periods of above-average precipitation and favorable temperatures–colder than mean annual temperatures in Spain–promote vigorous vegetation

growth that subsequently becomes vulnerable during drier and hotter conditions. Trees that expand their canopy and root systems during favorable periods can become structurally overbuilt relative to what local water availability can sustain long-term, creating a temporal mismatch between water demand and supply (Jump et al. 2017; Yao Zhang et al. 2021; Yixuan Zhang et al. 2024). When environmental favorability declines, this mismatch leads to intensified water stress, driving responses from premature leaf senescence to whole-tree mortality. This mechanism operates globally, with an estimated 11% of droughts during 1981-2015 being overshoot-related (Yao Zhang et al. 2021). Additionally, biomass accumulation in forest understories becomes fuel for wildfires during subsequent dry periods (Lecina-Diaz et al. 2014; Carnicer, Alegria, et al. 2022; Lian et al. 2024). Our model captured the largest carbon losses (12.9%) during the 2021-2022 transition, coinciding with the record 2022 drought that reduced European forest carbon uptake by 56-62 TgC (Woude et al. 2023) and a record year for burned area in Spain, with 315,705 hectares burned—three-and-a-half times more than in 2021 and representing the highest increase in burnt area among EU countries (San-Miguel-Ayanz et al. 2023)—a pattern consistent with structural overshoot vulnerability.

Our findings reveal that this mechanism operates at annual timescales and responds to interannual variability rather than solely to long-term climatic baselines. The critical factor is not the absolute magnitude of climate anomalies relative to the 30-year baseline, but rather the difference between accumulated and same-year conditions. Woody carbon losses occur when accumulated precipitation anomalies exceed same-year anomalies, regardless of whether both are positive or negative—indicating vulnerability during both prolonged drought periods and unusually wet periods. This suggests that structural overshoot can operate as a short-term dynamic process driven by year-to-year climate variability, irrespective of the climatic baseline in which forest ecosystems may have developed.

4.2 Species composition and forest structure drive varying responses

Our results revealed pronounced differences in carbon vulnerability across forest types, potentially reflecting both species-specific physiological traits and structural characteristics that determine resilience to the structural overshoot effect. We estimated that coniferous forests experienced the most substantial biomass carbon losses (21% decline), which may reflect both fundamental constraints of their hydraulic architecture and the structural characteristics of many Spanish conifer stands. These findings are consistent with established evidence of conifers' vulnerability to drought in Mediterranean systems (Carnicer, Barbeta, et al. 2013). Moreover, dense pine plantations show greater vulnerability to drought impacts than natural stands with more heterogeneous structures and lower density (Calama et al., 2024), with dense plantations in Mediterranean Spain experiencing higher defoliation and mortality under drought stress compared to lower-density stands (Sánchez-Salguero et al., 2013; Rodríguez-Vallejo et al., 2021). Additionally, conifers depend on long-lived needles that cannot be rapidly replaced following drought damage, creating legacy effects that may limit post-drought recovery (Song et al. 2022; Sterck et al. 2024).

We also found that *Eucalyptus* forests suffered severe biomass carbon losses (30%) during 2021-2022. Although *Eucalyptus* species are native to arid and semi-arid regions and well-adapted to water limitation, trees can reach very large sizes at fast growing speeds in conditions of high-water availability (Correia et al. 2014; Christina et al. 2017). In Spain, *Eucalyptus* forests are concentrated in the rainiest northwestern regions, where they were initially introduced as a productive species (Queirós et al. 2020), despite their often negative effects on water provision, soil quality and biodiversity (Jackson et al. 2005; Calviño-Cancela et al. 2012; Lemessa et al. 2022). Their fast growth in wet conditions likely makes *Eucalyptus* more vulnerable to structural overshoot, especially during severe summer droughts (Correia et al. 2014), with recent evidence showing their poor drought-resilience when compared to native species (Khoury and Coomes 2020). When it comes to fire, *Eucalyptus*' aggressive post-fire resprout capacity may enable its persistence and potential range expansion following disturbances (Catry et al. 2013).

In contrast, *Quercus*-dominated systems exhibited greater resilience (7.5% loss) and a faster recovery than conifers, probably reflecting their predominantly resprouting capacity and higher resilience to disturbances through vegetative regeneration (Pausas and Vallejo 1999; Pausas and Keeley 2014). For *Quercus ilex*, the dominant oak species in Spain, this resilience may also reflect evolutionary adaptations to Mediterranean conditions mainly herbivory, drought and disturbances (Pausas and Keeley 2014; Khoury and Coomes 2020). This differential response suggests that evolutionary history and local adaptation could be a key determinant of forest resilience and biomass carbon stock stability under increasing climate stress. However, other factors such as stand structure, functional diversity and understory dynamics likely also play a role in modulating this response.

Beyond species composition, we found that low-density woodlands and agroforestry systems–olive groves and orchards–experienced minimal losses (5%) over the same period. Their comparatively higher resilience likely reflects a combination of structural and management factors (e.g. Fernandes 2009), such as lower density (reducing competition for water and fire intensity and spread), active fuel load reduction, and, in some cases, supplemental irrigation.

4.3 Methodological consideration in interpreting biomass carbon losses

An important methodological consideration may influence the interpretation of the apparent shrubification pattern we observed. During drought-induced stress, deciduous species typically reduce leaf coverage and canopy density as an adaptive response (J.-F. Liu et al. 2017; Mariën et al. 2021), which directly alters the spectral signatures captured by Sentinel-2 imagery (Q. Liu et al. 2023). Since our CNN model infers height from multi-spectral signals, drought-induced reductions in leaf area may systematically bias height predictions toward lower values. Consequently, trees that have reduced foliage but retain intact stem biomass could appear in our analysis as having lost carbon, when the underlying woody structure remains present but threatened (Appendix S1: Figure S5). While our results capture genuine signals of forest vulnerability, this methodological consideration indicates that the total

magnitude of immediate carbon loss may be overestimated, and that predicted losses might be time-lagged (Appendix S1: Figure S5).

4.4 Management interventions: preventing structural overshoot

The structural overshoot dynamic identified creates a critical management challenge: how to maintain carbon storage while preventing dangerous fuel accumulation and increased stress due to competition for water. In the context of widespread land abandonment that has altered fire regimes across Mediterranean regions (Ursino and Romano 2014), thinning emerges as a primary adaptation strategy, enhancing drought resilience by reducing tree competition for limited water resources (Elkin et al. 2015; Sohn et al. 2016; Domingo et al. 2020; Zavala et al. 2024) and decreasing fire-prone fuel loads. Strategic grazing can complement thinning by diminishing understory biomass, reducing fuel loads and creating spatial heterogeneity in fuel distribution that mitigates wildfire risk (Starns et al. 2019; Rouet-Leduc et al. 2021; Pillar and Overbeck 2025). Herbivores, however, have limited reach for most woody material, requiring integrated approaches combining silviculture, prescribed fire, and targeted grazing. This integrated management approach aligns with fire-smart principles (Fernandes 2013) and can potentially support ecological restoration initiatives centered on rewilding (Araújo and Alagador 2024). Alternatively, extracting biomass for materials rather than allowing accumulation can serve as a mitigation strategy with lower emissions than prescribed fire or grazing (Bar-On et al. 2025). High-resolution satellite monitoring of forests, like the approach we implemented, can help identify areas where biomass accumulation may increase structural overshoot vulnerability, enabling more targeted management interventions.

5 Conclusions

Our findings demonstrate that climate change is already undermining woody carbon storage capacity in Mediterranean regions, with Spanish forests and woodlands functioning as net carbon sources over the past 5 years. This pattern potentially foreshadows similar challenges

across Mediterranean ecosystems in southern Europe, where climate projections indicate intensifying aridity and increasing temperature extremes. Recent analysis shows that despite less extreme meteorological conditions in 2022 compared to previous drought years, European forests experienced greater canopy damage, highlighting declining forest resilience over time (Woude et al. 2023; Gharun et al. 2024) . In contrast, many areas within Spanish Eurosiberian regions showed carbon gains, functioning as carbon sinks, particularly *Fagus sylvatica* forests, whereas *Eucalyptus* plantations experienced losses even in these regions. This suggests that Spanish Eurosiberian forests may maintain, or even increase, sink capacity with appropriate species composition.

Our methodological approach—combining deep learning with multi-source remote sensing data to create the most up-to-date high-resolution carbon density time-series for Spain—reveals that the capacity of forests as nature-based climate solutions is severely limited and threatened by climate change, challenging recent estimates (Keith et al. 2024). The structural overshoot mechanism we identified here probably operates in other ecosystems worldwide, suggesting that current climate mitigation strategies may systematically overestimate the stability of the carbon sink of forests (Chen et al. 2024). As most continental Spanish forests and woodlands transition from carbon sinks to sources, our work serves as a warning that achieving climate mitigation targets will require more aggressive emissions reductions than currently planned, and forest-based solutions alone might not be relied upon under accelerating climate change.

Acknowledgments

Funding was provided by the Spanish Ministry for the Ecological Transition and Demographic Challenge to the CSIC through project 20233TE007 for the preparation of technical documents supporting biodiversity protection against climate change (Art. 24, Law 7/2021).

Conflict of Interest Statement

The authors declare no conflict of interest.

Open research statement

All the code needed to reproduce the analysis and relevant data produced during the execution of the method is made publicly available in the Zenodo repository `https://zenodo.org/records/15755780`. Code is also available in the GitHub repository `https://github.com/diegomvd/carbon_dynamics_spain`.

References

Alibakhshi, Sara et al. (Oct. 10, 2024). "Natural forest regeneration is projected to reduce local temperatures". In: *Communications Earth & Environment* 5.1. Publisher: Nature Publishing Group, p. 577. ISSN: 2662-4435. DOI: 10.1038/s43247-024-01737-5. URL: https://www.nature.com/articles/s43247-024-01737-5 (visited on 06/16/2025).

Araújo, Miguel B. and Diogo Alagador (Sept. 9, 2024). "Expanding European protected areas through rewilding". In: *Current Biology* 34.17. Publisher: Elsevier, 3931–3940.e5. ISSN: 0960-9822. DOI: 10.1016/j.cub.2024.07.045. URL: https://www.cell.com/current-biology/abstract/S0960-9822(24)00948-5 (visited on 06/17/2025).

Araújo, Miguel B., Richard G. Pearson, et al. (2005). "Validation of species–climate impact models under climate change". In: *Global Change Biology* 11.9. _eprint: https://onlinelibrary.wiley.com/doi/pdf/10.1111/j.1365-2486.2005.01000.x, pp. 1504–1513. ISSN: 1365-2486. DOI: 10.1111/j.1365-2486.2005.01000.x. URL: https://onlinelibrary.wiley.com/doi/abs/10.1111/j.1365-2486.2005.01000.x (visited on 06/16/2025).

Ball, John E., Derek T. Anderson, and Chee Seng Chan Sr (Sept. 2017). "Comprehensive survey of deep learning in remote sensing: theories, tools, and challenges for the community".

In: *Journal of Applied Remote Sensing* 11.4. Publisher: SPIE, p. 042609. ISSN: 1931-3195, 1931-3195. DOI: 10.1117/1.JRS.11.042609. URL: https://www.spiedigitallibrary.org/journals/journal-of-applied-remote-sensing/volume-11/issue-4/042609/Comprehensive-survey-of-deep-learning-in-remote-sensing--theories/10.1117/1.JRS.11.042609.full (visited on 06/17/2025).

Bar-On, Yinon M. et al. (Mar. 21, 2025). "Recent gains in global terrestrial carbon stocks are mostly stored in nonliving pools". In: *Science* 387.6740. Publisher: American Association for the Advancement of Science, pp. 1291–1295. DOI: 10.1126/science.adk1637. URL: https://www.science.org/doi/10.1126/science.adk1637 (visited on 06/17/2025).

Booth, Trevor H. (2022). "Checking bioclimatic variables that combine temperature and precipitation data before their use in species distribution models". In: *Austral Ecology* 47.7. _eprint: https://onlinelibrary.wiley.com/doi/pdf/10.1111/aec.13234, pp. 1506–1514. ISSN: 1442-9993. DOI: 10.1111/aec.13234. URL: https://onlinelibrary.wiley.com/doi/abs/10.1111/aec.13234 (visited on 06/16/2025).

Breiman, Leo (Oct. 1, 2001). "Random Forests". In: *Machine Learning* 45.1, pp. 5–32. ISSN: 1573-0565. DOI: 10.1023/A:1010933404324. URL: https://doi.org/10.1023/A:1010933404324 (visited on 06/16/2025).

Calviño-Cancela, María, Margarita Rubido-Bará, and Eddie J. B. van Etten (Apr. 15, 2012). "Do eucalypt plantations provide habitat for native forest biodiversity?" In: *Forest Ecology and Management* 270, pp. 153–162. ISSN: 0378-1127. DOI: 10.1016/j.foreco.2012.01.019. URL: https://www.sciencedirect.com/science/article/pii/S0378112712000291 (visited on 06/16/2025).

Carnicer, Jofre, Andrés Alegria, et al. (June 20, 2022). "Global warming is shifting the relationships between fire weather and realized fire-induced CO2 emissions in Europe". In: *Scientific Reports* 12.1. Publisher: Nature Publishing Group, p. 10365. ISSN: 2045-2322. DOI: 10.1038/s41598-022-14480-8. URL: https://www.nature.com/articles/s41598-022-14480-8 (visited on 06/16/2025).

Carnicer, Jofre, Adria Barbeta, et al. (Oct. 17, 2013). "Contrasting trait syndromes in angiosperms and conifers are associated with different responses of tree growth to temperature on a large scale". In: *Frontiers in Plant Science* 4. Publisher: Frontiers. ISSN:

1664-462X. DOI: 10.3389/fpls.2013.00409. URL: https://www.frontiersin.org/journals/plant-science/articles/10.3389/fpls.2013.00409/full (visited on 06/16/2025).

Carnicer, Jofre, Marta Coll, et al. (Jan. 25, 2011). "Widespread crown condition decline, food web disruption, and amplified tree mortality with increased climate change-type drought". In: *Proceedings of the National Academy of Sciences* 108.4, pp. 1474–1478. ISSN: 0027-8424, 1091-6490. DOI: 10.1073/pnas.1010070108. URL: https://pnas.org/doi/full/10.1073/pnas.1010070108 (visited on 06/16/2025).

Catry, Filipe X. et al. (Dec. 15, 2013). "Post-fire survival and regeneration of *Eucalyptus globulus* in forest plantations in Portugal". In: *Forest Ecology and Management* 310, pp. 194–203. ISSN: 0378-1127. DOI: 10.1016/j.foreco.2013.08.036. URL: https://www.sciencedirect.com/science/article/pii/S037811271300563X (visited on 06/16/2025).

Chave, Jerome et al. (2009). "Towards a worldwide wood economics spectrum". In: *Ecology Letters* 12.4. _eprint: https://onlinelibrary.wiley.com/doi/pdf/10.1111/j.1461-0248.2009.01285.x, pp. 351–366. ISSN: 1461-0248. DOI: 10.1111/j.1461-0248.2009.01285.x. URL: https://onlinelibrary.wiley.com/doi/abs/10.1111/j.1461-0248.2009.01285.x (visited on 03/27/2025).

Chen, Yi-Ying et al. (Feb. 2024). "When forests hold their breath: will increasing drought further disrupt carbon sequestration?" In: *Environmental Research Letters* 19.3. Publisher: IOP Publishing, p. 031002. ISSN: 1748-9326. DOI: 10.1088/1748-9326/ad27ba. URL: https://dx.doi.org/10.1088/1748-9326/ad27ba (visited on 06/16/2025).

Chiti, Tommaso et al. (Oct. 16, 2024). *Carbon farming in the European forestry sector*. From Science to Policy. Series: From Science to Policy. European Forest Institute. DOI: 10.36333/fs17. URL: https://efi.int/publications-bank/carbon-farming-european-forestry-sector (visited on 01/31/2025).

Christina, Mathias et al. (2017). "Importance of deep water uptake in tropical eucalypt forest". In: *Functional Ecology* 31.2. _eprint: https://besjournals.onlinelibrary.wiley.com/doi/pdf/10.1111/2435.12727, pp. 509–519. ISSN: 1365-2435. DOI: 10.1111/1365-2435.12727. URL: https:

//onlinelibrary.wiley.com/doi/abs/10.1111/1365-2435.12727 (visited on 06/16/2025).

Copernicus Land Monitoring Service (2020). *CORINE Land Cover 2018*. DOI: 10.2909/960998c1-1870-4e82-8051-6485205ebbac. (Visited on 02/24/2025).

Copernicus Sentinel data (2024). *Sentinel-2 Level-2A Collection*. Earth Search STAC API. URL: https://earth-search.aws.element84.com/v1 (visited on 09/15/2024).

Correia, Barbara et al. (2014). "Water stress and recovery in the performance of two Eucalyptus globulus clones: physiological and biochemical profiles". In: *Physiologia Plantarum* 150.4. _eprint: https://onlinelibrary.wiley.com/doi/pdf/10.1111/ppl.12110, pp. 580–592. ISSN: 1399-3054. DOI: 10.1111/ppl.12110. URL: https://onlinelibrary.wiley.com/doi/abs/10.1111/ppl.12110 (visited on 06/16/2025).

Dasari, Hari Prasad et al. (Nov. 17, 2014). "A Regional Climate Study of Heat Waves over the Iberian Peninsula". In: *Atmospheric and Climate Sciences* 4.5. Number: 5 Publisher: Scientific Research Publishing, pp. 841–853. DOI: 10.4236/acs.2014.45074. URL: https://www.scirp.org/journal/paperinformation?paperid=51589 (visited on 06/17/2025).

Directorate-General for Communication (European Commission) (2021). *European green deal: delivering on our targets*. Publications Office of the European Union. ISBN: 978-92-76-39487-7. URL: https://data.europa.eu/doi/10.2775/595210 (visited on 06/16/2025).

Domingo, Jose, Miguel A. Zavala, and Jaime Madrigal-González (July 1, 2020). "Thinning enhances stool resistance to an extreme drought in a Mediterranean Quercus ilex L. coppice: insights for adaptation". In: *New Forests* 51.4, pp. 597–613. ISSN: 1573-5095. DOI: 10.1007/s11056-019-09755-4. URL: https://doi.org/10.1007/s11056-019-09755-4 (visited on 06/17/2025).

Duncanson, Laura et al. (Mar. 1, 2022). "Aboveground biomass density models for NASA's Global Ecosystem Dynamics Investigation (GEDI) lidar mission". In: *Remote Sensing of Environment* 270, p. 112845. ISSN: 0034-4257. DOI: 10.1016/j.rse.2021.112845. URL: https://www.sciencedirect.com/science/article/pii/S0034425721005654 (visited on 02/29/2024).

Elkin, Ché et al. (2015). "Short- and long-term efficacy of forest thinning to mitigate drought impacts in mountain forests in the European Alps". In: *Ecological Applications* 25.4. _eprint: https://esajournals.onlinelibrary.wiley.com/doi/pdf/10.1890/14-0690.1, pp. 1083–1098. ISSN: 1939-5582. DOI: 10.1890/14-0690.1. URL: https://onlinelibrary.wiley.com/doi/abs/10.1890/14-0690.1 (visited on 06/17/2025).

Felipe-Lucia, María R. et al. (Nov. 16, 2018). "Multiple forest attributes underpin the supply of multiple ecosystem services". In: *Nature Communications* 9.1. Publisher: Nature Publishing Group, p. 4839. ISSN: 2041-1723. DOI: 10.1038/s41467-018-07082-4. URL: https://www.nature.com/articles/s41467-018-07082-4 (visited on 06/16/2025).

Fernandes, Paulo M. (Jan. 2009). "Combining forest structure data and fuel modelling to classify fire hazard in Portugal". In: *Annals of Forest Science* 66.4. Number: 4 Publisher: BioMed Central, pp. 415–415. ISSN: 1297-966X. DOI: 10.1051/forest/2009013. URL: https://annforsci.biomedcentral.com/articles/10.1051/forest/2009013 (visited on 06/16/2025).

— (Feb. 1, 2013). "Fire-smart management of forest landscapes in the Mediterranean basin under global change". In: *Landscape and Urban Planning* 110, pp. 175–182. ISSN: 0169-2046. DOI: 10.1016/j.landurbplan.2012.10.014. URL: https://www.sciencedirect.com/science/article/pii/S0169204612002952 (visited on 06/16/2025).

Forzieri, Giovanni et al. (Feb. 23, 2021). "Emergent vulnerability to climate-driven disturbances in European forests". In: *Nature Communications* 12.1. Publisher: Nature Publishing Group, p. 1081. ISSN: 2041-1723. DOI: 10.1038/s41467-021-21399-7. URL: https://www.nature.com/articles/s41467-021-21399-7 (visited on 03/27/2025).

García-Valdés, Raúl, Jens-Christian Svenning, et al. (2015). "Evaluating the combined effects of climate and land-use change on tree species distributions". In: *Journal of Applied Ecology* 52.4. _eprint: https://besjournals.onlinelibrary.wiley.com/doi/pdf/10.1111/1365-2664.12453, pp. 902–912. ISSN: 1365-2664. DOI: 10.1111/1365-2664.12453. URL: https://onlinelibrary.wiley.com/doi/abs/10.1111/1365-2664.12453 (visited on 06/17/2025).

García-Valdés, Raúl, Miguel A. Zavala, et al. (2013). "Chasing a moving target: projecting climate change-induced shifts in non-equilibrial tree species distributions". In: *Journal of Ecology* 101.2. _eprint: https://besjournals.onlinelibrary.wiley.com/doi/pdf/10.1111/1365-

2745.12049, pp. 441–453. ISSN: 1365-2745. DOI: 10.1111/1365-2745.12049. URL: https://onlinelibrary.wiley.com/doi/abs/10.1111/1365-2745.12049 (visited on 06/17/2025).

George, Darren and Paul Mallery (Dec. 6, 2019). *IBM SPSS Statistics 26 Step by Step: A Simple Guide and Reference*. 16th ed. New York: Routledge. 402 pp. ISBN: 978-0-429-05676-5. DOI: 10.4324/9780429056765.

Gharun, Mana et al. (Dec. 11, 2024). "Effect of the 2022 summer drought across forest types in Europe". In: *Biogeosciences* 21.23. Publisher: Copernicus GmbH, pp. 5481–5494. ISSN: 1726-4170. DOI: 10.5194/bg-21-5481-2024. URL: https://bg.copernicus.org/articles/21/5481/2024/ (visited on 06/16/2025).

Guo, Wenwen et al. (2025). "Global Critical Drought Thresholds of Terrestrial Carbon Sink–Source Transition". In: *Global Change Biology* 31.3. _eprint: https://onlinelibrary.wiley.com/doi/p e70129. ISSN: 1365-2486. DOI: 10.1111/gcb.70129. URL: https://onlinelibrary.wiley.com/doi/abs/10.1111/gcb.70129 (visited on 03/27/2025).

Instituto Geográfico Nacional (2021). *PNOA LiDAR*. Plan Nacional de Ortofotografía Aérea, PNOA LiDAR. URL: https://pnoa.ign.es/web/portal/pnoa-lidar/presentacion (visited on 07/12/2024).

Jackson, Robert B. et al. (Dec. 23, 2005). "Trading Water for Carbon with Biological Carbon Sequestration". In: *Science* 310.5756. Publisher: American Association for the Advancement of Science, pp. 1944–1947. DOI: 10.1126/science.1119282. URL: https://www.science.org/doi/10.1126/science.1119282 (visited on 06/17/2025).

Jump, Alistair S. et al. (2017). "Structural overshoot of tree growth with climate variability and the global spectrum of drought-induced forest dieback". In: *Global Change Biology* 23.9. _eprint: https://onlinelibrary.wiley.com/doi/pdf/10.1111/gcb.13636, pp. 3742–3757. ISSN: 1365-2486. DOI: 10.1111/gcb.13636. URL: https://onlinelibrary.wiley.com/doi/abs/10.1111/gcb.13636 (visited on 06/16/2025).

Keith, Heather et al. (May 14, 2024). "Carbon carrying capacity in primary forests shows potential for mitigation achieving the European Green Deal 2030 target". In: *Communications Earth & Environment* 5.1. Publisher: Nature Publishing Group, p. 256. ISSN:

2662-4435. DOI: 10.1038/s43247-024-01416-5. URL: https://www.nature.com/articles/s43247-024-01416-5 (visited on 06/16/2025).

Khoury, Sacha and David A. Coomes (2020). "Resilience of Spanish forests to recent droughts and climate change". In: *Global Change Biology* 26.12. _eprint: https://onlinelibrary.wiley.com/doi/pdf/ pp. 7079–7098. ISSN: 1365-2486. DOI: 10.1111/gcb.15268. URL: https://onlinelibrary.wiley.com/doi/abs/10.1111/gcb.15268 (visited on 06/16/2025).

Lang, Nico, Walter Jetz, et al. (Nov. 2023). "A high-resolution canopy height model of the Earth". In: *Nature Ecology & Evolution* 7.11. Publisher: Nature Publishing Group, pp. 1778–1789. ISSN: 2397-334X. DOI: 10.1038/s41559-023-02206-6. URL: https://www.nature.com/articles/s41559-023-02206-6 (visited on 11/11/2024).

Lang, Nico, Konrad Schindler, and Jan Dirk Wegner (Nov. 1, 2019). "Country-wide high-resolution vegetation height mapping with Sentinel-2". In: *Remote Sensing of Environment* 233, p. 111347. ISSN: 0034-4257. DOI: 10.1016/j.rse.2019.111347. URL: https://www.sciencedirect.com/science/article/pii/S0034425719303669 (visited on 09/12/2024).

Lazoglou, Georgia et al. (Sept. 2024). "Climate change and extremes in the Mediterranean island of Cyprus: from historical trends to future projections". In: *Environmental Research Communications* 6.9. Publisher: IOP Publishing, p. 095020. ISSN: 2515-7620. DOI: 10.1088/2515-7620/ad7927. URL: https://dx.doi.org/10.1088/2515-7620/ad7927 (visited on 03/27/2025).

Lecina-Diaz, Judit, Albert Alvarez, and Javier Retana (Jan. 22, 2014). "Extreme Fire Severity Patterns in Topographic, Convective and Wind-Driven Historical Wildfires of Mediterranean Pine Forests". In: *PLOS ONE* 9.1. Publisher: Public Library of Science, e85127. ISSN: 1932-6203. DOI: 10.1371/journal.pone.0085127. URL: https://journals.plos.org/plosone/article?id=10.1371/journal.pone.0085127 (visited on 06/16/2025).

Lemessa, Debissa et al. (Nov. 1, 2022). "Do *Eucalyptus* plantation forests support biodiversity conservation?" In: *Forest Ecology and Management* 523, p. 120492. ISSN: 0378-1127. DOI: 10.1016/j.foreco.2022.120492. URL: https://www.sciencedirect.com/science/article/pii/S0378112722004868 (visited on 06/16/2025).

Lian, Xu et al. (Feb. 2024). "Diminishing carryover benefits of earlier spring vegetation growth". In: *Nature Ecology & Evolution* 8.2. Publisher: Nature Publishing Group, pp. 218–228. ISSN: 2397-334X. DOI: 10.1038/s41559-023-02272-w. URL: https://www.nature.com/articles/s41559-023-02272-w (visited on 06/16/2025).

Lipovetsky, Stan and Michael Conklin (2001). "Analysis of regression in game theory approach". In: *Applied Stochastic Models in Business and Industry* 17.4. _eprint: https://onlinelibrary.wile pp. 319–330. ISSN: 1526-4025. DOI: 10.1002/asmb.446. URL: https://onlinelibrary.wiley.com/doi/abs/10.1002/asmb.446 (visited on 06/16/2025).

Liu, Jian-Feng et al. (Feb. 14, 2017). "Effects of drought on leaf carbon source and growth of European beech are modulated by soil type". In: *Scientific Reports* 7.1. Publisher: Nature Publishing Group, p. 42462. ISSN: 2045-2322. DOI: 10.1038/srep42462. URL: https://www.nature.com/articles/srep42462 (visited on 06/16/2025).

Liu, Qi et al. (June 1, 2023). "The response and sensitivity of global vegetation to water stress: A comparison of different satellite-based NDVI products". In: *International Journal of Applied Earth Observation and Geoinformation* 120, p. 103341. ISSN: 1569-8432. DOI: 10.1016/j.jag.2023.103341. URL: https://www.sciencedirect.com/science/article/pii/S1569843223001632 (visited on 06/16/2025).

Loidi, Javier and Denys Vynokurov (May 20, 2024). "The biogeographical kingdoms and regions of the world". In: *Mediterranean Botany* 45.2. Number: 2, e92333–e92333. ISSN: 2603-9109. DOI: 10.5209/mbot.92333. URL: https://revistas.ucm.es/index.php/MBOT/article/view/92333 (visited on 06/16/2025).

Lundberg, Scott (2017). "A unified approach to interpreting model predictions". In: *arXiv preprint arXiv:1705.07874*.

Mariën, Bertold et al. (June 4, 2021). "Does drought advance the onset of autumn leaf senescence in temperate deciduous forest trees?" In: *Biogeosciences* 18.11. Publisher: Copernicus GmbH, pp. 3309–3330. ISSN: 1726-4170. DOI: 10.5194/bg-18-3309-2021. URL: https://bg.copernicus.org/articles/18/3309/2021/ (visited on 06/16/2025).

Ministerio para la Transición Ecológica y el Reto Demográfico (2025a). *Cuarto Inventario Forestal Nacional (NFI4)*. Ministerio para la Transición Ecológica y el Reto Demográfico. URL: https://www.miteco.gob.es/es/biodiversidad/temas/inventarios-

nacionales/inventario-forestal-nacional/cuarto_inventario.html (visited on 06/10/2024).

Ministerio para la Transición Ecológica y el Reto Demográfico (2025b). *Mapa Forestal de España (MFE 25)*. Ministerio para la Transición Ecológica y el Reto Demográfico. URL: https://www.miteco.gob.es/es/cartografia-y-sig/ide/descargas/biodiversidad/mfe.html (visited on 06/28/2024).

Muñoz Sabater, Joaquín (2019). *ERA5-Land monthly averaged data from 1950 to present*. DOI: 10.24381/cds.68d2bb30. (Visited on 03/02/2025).

Nabuurs, Gert-Jan et al. (Sept. 2013). "First signs of carbon sink saturation in European forest biomass". In: *Nature Climate Change* 3.9. Publisher: Nature Publishing Group, pp. 792–796. ISSN: 1758-6798. DOI: 10.1038/nclimate1853. URL: https://www.nature.com/articles/nclimate1853 (visited on 06/16/2025).

Pan, Yude et al. (July 2024). "The enduring world forest carbon sink". In: *Nature* 631.8021. Publisher: Nature Publishing Group, pp. 563–569. ISSN: 1476-4687. DOI: 10.1038/s41586-024-07602-x. URL: https://www.nature.com/articles/s41586-024-07602-x (visited on 06/16/2025).

Patacca, Marco et al. (2023). "Significant increase in natural disturbance impacts on European forests since 1950". In: *Global Change Biology* 29.5. _eprint: https://onlinelibrary.wiley.com/doi/pd pp. 1359–1376. ISSN: 1365-2486. DOI: 10.1111/gcb.16531. URL: https://onlinelibrary.wiley.com/doi/abs/10.1111/gcb.16531 (visited on 06/16/2025).

Pausas, Juli G. and Jon E. Keeley (2014). "Evolutionary ecology of resprouting and seeding in fire-prone ecosystems". In: *New Phytologist* 204.1. _eprint: https://nph.onlinelibrary.wiley.com/doi/pdf/ pp. 55–65. ISSN: 1469-8137. DOI: 10.1111/nph.12921. URL: https://onlinelibrary.wiley.com/doi/abs/10.1111/nph.12921 (visited on 06/16/2025).

Pausas, Juli G. and V. Ramón Vallejo (1999). "The role of fire in European Mediterranean ecosystems". In: *Remote Sensing of Large Wildfires: in the European Mediterranean Basin*. Ed. by Emilio Chuvieco. Berlin, Heidelberg: Springer, pp. 3–16. ISBN: 978-3-642-60164-4. DOI: 10.1007/978-3-642-60164-4_2. URL: https://doi.org/10.1007/978-3-642-60164-4_2 (visited on 06/17/2025).

Pedregosa, Fabian et al. (Nov. 1, 2011). "Scikit-learn: Machine Learning in Python". In: *The Journal of Machine Learning Research* 12 (null), pp. 2825–2830. ISSN: 1532-4435.

Peñuelas, Josep et al. (Oct. 2017). "Shifting from a fertilization-dominated to a warming-dominated period". In: *Nature Ecology & Evolution* 1.10. Publisher: Nature Publishing Group, pp. 1438–1445. ISSN: 2397-334X. DOI: 10.1038/s41559-017-0274-8. URL: https://www.nature.com/articles/s41559-017-0274-8 (visited on 03/27/2025).

Pillar, Valério D. and Gerhard E. Overbeck (Jan. 9, 2025). "Grazing can reduce wildfire risk amid climate change". In: *Science* 387.6730. Publisher: American Association for the Advancement of Science, eadu7471. DOI: 10.1126/science.adu7471. URL: https://www.science.org/doi/full/10.1126/science.adu7471 (visited on 06/16/2025).

Queirós, L. et al. (June 15, 2020). "Assessing the drivers and the recruitment potential of *Eucalyptus globulus* in the Iberian Peninsula". In: *Forest Ecology and Management* 466, p. 118147. ISSN: 0378-1127. DOI: 10.1016/j.foreco.2020.118147. URL: https://www.sciencedirect.com/science/article/pii/S037811271932626X (visited on 06/16/2025).

Ronneberger, Olaf, Philipp Fischer, and Thomas Brox (2015). "U-Net: Convolutional Networks for Biomedical Image Segmentation". In: *Medical Image Computing and Computer-Assisted Intervention – MICCAI 2015*. Ed. by Nassir Navab et al. Cham: Springer International Publishing, pp. 234–241. ISBN: 978-3-319-24574-4. DOI: 10.1007/978-3-319-24574-4_28.

Rouet-Leduc, Julia et al. (2021). "Effects of large herbivores on fire regimes and wildfire mitigation". In: *Journal of Applied Ecology* 58.12. _eprint: https://besjournals.onlinelibrary.wiley.com/doi/p 2664.13972, pp. 2690–2702. ISSN: 1365-2664. DOI: 10.1111/1365-2664.13972. URL: https://onlinelibrary.wiley.com/doi/abs/10.1111/1365-2664.13972 (visited on 06/16/2025).

San-Miguel-Ayanz, Jesús et al. (2023). *Advance report on forest fires in Europe, Middle East and North Africa 2022*. Publications Office of the European Union. ISBN: 978-92-68-02143-9. URL: https://data.europa.eu/doi/10.2760/091540 (visited on 06/17/2025).

Schwartz, Martin et al. (Nov. 2, 2023). "FORMS: Forest Multiple Source height, wood volume, and biomass maps in France at 10 to 30 m resolution based on Sentinel-1, Sentinel-

2, and Global Ecosystem Dynamics Investigation (GEDI) data with a deep learning approach". In: *Earth System Science Data* 15.11, pp. 4927–4945. ISSN: 1866-3516. DOI: 10.5194/essd-15-4927-2023. URL: https://essd.copernicus.org/articles/15/4927/2023/ (visited on 02/29/2024).

Shah, Syed Aamir Ali, Muhammad Asif Manzoor, and Abdul Bais (Mar. 2020). "Canopy Height Estimation at Landsat Resolution Using Convolutional Neural Networks". In: *Machine Learning and Knowledge Extraction* 2.1. Number: 1 Publisher: Multidisciplinary Digital Publishing Institute, pp. 23–36. ISSN: 2504-4990. DOI: 10.3390/make2010003. URL: https://www.mdpi.com/2504-4990/2/1/3 (visited on 06/17/2025).

Shanley, Colin S. et al. (Sept. 12, 2024). "Mapping forest-based natural climate solutions". In: *Communications Earth & Environment* 5.1. Publisher: Nature Publishing Group, pp. 1–12. ISSN: 2662-4435. DOI: 10.1038/s43247-024-01678-z. URL: https://www.nature.com/articles/s43247-024-01678-z (visited on 03/27/2025).

Smith, Leslie N. and Nicholay Topin (Aug. 23, 2017). *Super-Convergence: Very Fast Training of Neural Networks Using Large Learning Rates*. arXiv.org. URL: https://arxiv.org/abs/1708.07120v3 (visited on 06/16/2025).

Sohn, Julia A., Somidh Saha, and Jürgen Bauhus (Nov. 15, 2016). "Potential of forest thinning to mitigate drought stress: A meta-analysis". In: *Forest Ecology and Management*. Special section: Drought and US Forests: Impacts and Potential Management Responses 380, pp. 261–273. ISSN: 0378-1127. DOI: 10.1016/j.foreco.2016.07.046. URL: https://www.sciencedirect.com/science/article/pii/S0378112716304029 (visited on 06/17/2025).

Song, Yanjun et al. (2022). "Drought resilience of conifer species is driven by leaf lifespan but not by hydraulic traits". In: *New Phytologist* 235.3. _eprint: https://nph.onlinelibrary.wiley.com/doi/pdf pp. 978–992. ISSN: 1469-8137. DOI: 10.1111/nph.18177. URL: https://onlinelibrary.wiley.com/doi/abs/10.1111/nph.18177 (visited on 06/16/2025).

Starns, Heath D. et al. (2019). "Recoupling fire and grazing reduces wildland fuel loads on rangelands". In: *Ecosphere* 10.1. _eprint: https://esajournals.onlinelibrary.wiley.com/doi/pdf/10.1002/e e02578. ISSN: 2150-8925. DOI: 10.1002/ecs2.2578. URL: https://onlinelibrary.wiley.com/doi/abs/10.1002/ecs2.2578 (visited on 06/16/2025).

Sterck, Frank J., Yanjun Song, and Lourens Poorter (Apr. 12, 2024). "Drought- and heat-induced mortality of conifer trees is explained by leaf and growth legacies". In: *Science Advances* 10.15. Publisher: American Association for the Advancement of Science, eadl4800. DOI: 10.1126/sciadv.adl4800. URL: https://www.science.org/doi/full/10.1126/sciadv.adl4800 (visited on 06/16/2025).

Štrumbelj, Erik and Igor Kononenko (Dec. 1, 2014). "Explaining prediction models and individual predictions with feature contributions". In: *Knowledge and Information Systems* 41.3, pp. 647–665. ISSN: 0219-3116. DOI: 10.1007/s10115-013-0679-x. URL: https://doi.org/10.1007/s10115-013-0679-x (visited on 06/16/2025).

Su, Yang et al. (Apr. 22, 2025). "Canopy height and biomass distribution across the forests of Iberian Peninsula". In: *Scientific Data* 12.1. Publisher: Nature Publishing Group, p. 678. ISSN: 2052-4463. DOI: 10.1038/s41597-025-05021-9. URL: https://www.nature.com/articles/s41597-025-05021-9 (visited on 06/16/2025).

Tan, Mingxing and Quoc Le (May 24, 2019). "EfficientNet: Rethinking Model Scaling for Convolutional Neural Networks". In: *Proceedings of the 36th International Conference on Machine Learning*. International Conference on Machine Learning. ISSN: 2640-3498. PMLR, pp. 6105–6114. URL: https://proceedings.mlr.press/v97/tan19a.html (visited on 03/27/2025).

Tanase, M. A. et al. (Oct. 15, 2024). "Long-term annual estimation of forest above ground biomass, canopy cover, and height from airborne and spaceborne sensors synergies in the Iberian Peninsula". In: *Environmental Research* 259, p. 119432. ISSN: 0013-9351. DOI: 10.1016/j.envres.2024.119432. URL: https://www.sciencedirect.com/science/article/pii/S0013935124013379 (visited on 11/11/2024).

Ursino, Nadia and Nunzio Romano (2014). "Wild forest fire regime following land abandonment in the Mediterranean region". In: *Geophysical Research Letters* 41.23. _eprint: https://agupubs.onlinelibrary.wiley.com/doi/pdf/10.1002/2014GL061560, pp. 8359–8368. ISSN: 1944-8007. DOI: 10.1002/2014GL061560. URL: https://onlinelibrary.wiley.com/doi/abs/10.1002/2014GL061560 (visited on 06/17/2025).

Vicente-Serrano, Sergio M et al. (Apr. 2014). "Evidence of increasing drought severity caused by temperature rise in southern Europe". In: *Environmental Research Letters* 9.4. Pub-

lisher: IOP Publishing, p. 044001. ISSN: 1748-9326. DOI: 10.1088/1748-9326/9/4/044001. URL: https://dx.doi.org/10.1088/1748-9326/9/4/044001 (visited on 03/27/2025).

Wang, Songhan et al. (Dec. 11, 2020). "Recent global decline of CO2 fertilization effects on vegetation photosynthesis". In: *Science* 370.6522. Publisher: American Association for the Advancement of Science, pp. 1295–1300. DOI: 10.1126/science.abb7772. URL: https://www.science.org/doi/10.1126/science.abb7772 (visited on 06/16/2025).

Wessely, Johannes et al. (June 2024). "A climate-induced tree species bottleneck for forest management in Europe". In: *Nature Ecology & Evolution* 8.6. Publisher: Nature Publishing Group, pp. 1109–1117. ISSN: 2397-334X. DOI: 10.1038/s41559-024-02406-8. URL: https://www.nature.com/articles/s41559-024-02406-8 (visited on 03/27/2025).

Woude, Auke M. van der et al. (Oct. 6, 2023). "Temperature extremes of 2022 reduced carbon uptake by forests in Europe". In: *Nature Communications* 14.1. Publisher: Nature Publishing Group, p. 6218. ISSN: 2041-1723. DOI: 10.1038/s41467-023-41851-0. URL: https://www.nature.com/articles/s41467-023-41851-0 (visited on 06/16/2025).

Zavala, Miguel A. et al. (Jan. 23, 2024). "Scaling up tree growth to assess forest resilience under increasing aridity: the case of Iberian dry-edge pine forests". In: *Landscape Ecology* 39.1, p. 6. ISSN: 1572-9761. DOI: 10.1007/s10980-024-01792-5. URL: https://doi.org/10.1007/s10980-024-01792-5 (visited on 06/17/2025).

Zhang, Yao, Trevor F. Keenan, and Sha Zhou (Nov. 2021). "Exacerbated drought impacts on global ecosystems due to structural overshoot". In: *Nature Ecology & Evolution* 5.11. Publisher: Nature Publishing Group, pp. 1490–1498. ISSN: 2397-334X. DOI: 10.1038/s41559-021-01551-8. URL: https://www.nature.com/articles/s41559-021-01551-8 (visited on 06/16/2025).

Zhang, Yixuan et al. (2024). "Intensified Structural Overshoot Aggravates Drought Impacts on Dryland Ecosystems". In: *Earth's Future* 12.1. _eprint: https://agupubs.onlinelibrary.wiley.com/doi/e2023EF003977. ISSN: 2328-4277. DOI: 10.1029/2023EF003977. URL: https://onlinelibrary.wiley.com/doi/abs/10.1029/2023EF003977 (visited on 06/16/2025).

Supporting Information

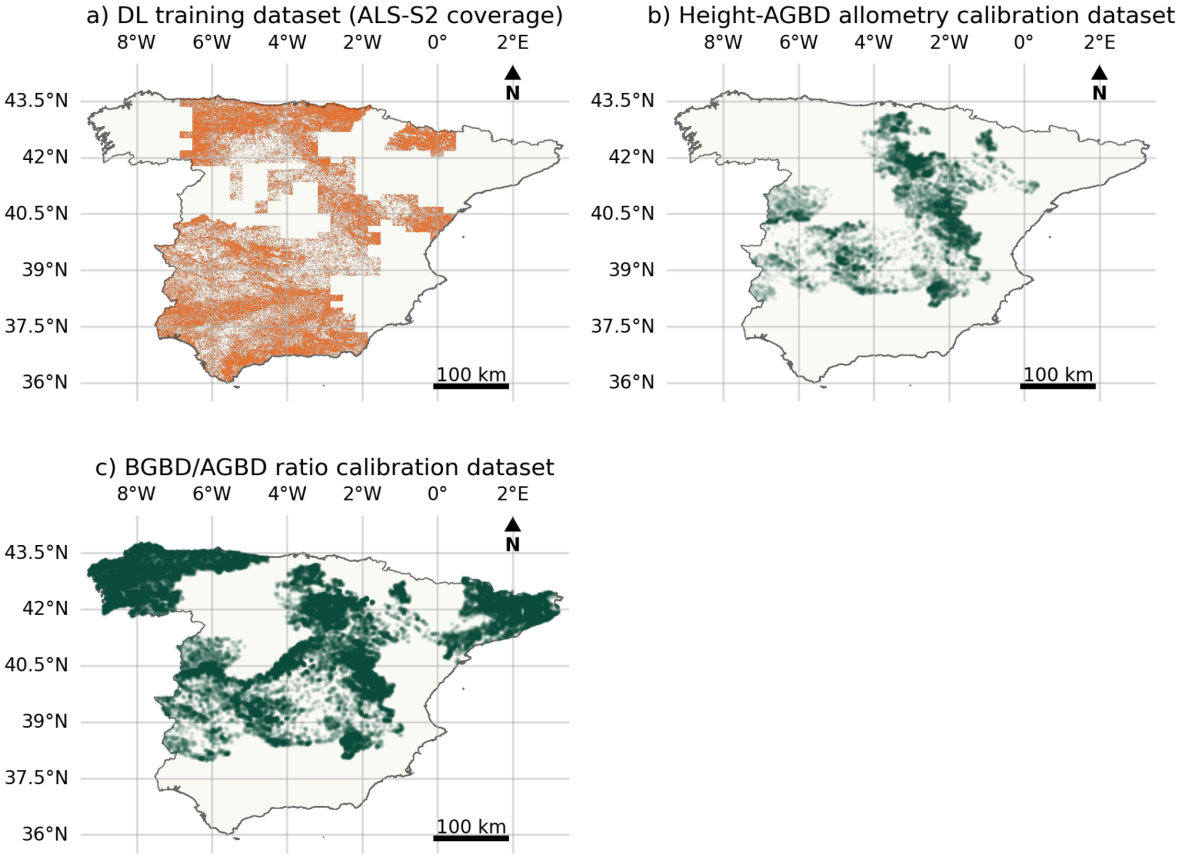

Figure S1. Data coverage. Geographic coverage of datasets used in this study: a) Training data for CNN-based canopy height inference from satellite imagery (163,094 km²), and field sample locations for allometric calibrations of b) canopy height-AGBD relationships (13,918 samples) and c) BGBD/AGBD ratios from national forest inventory plots (66,292 samples). Sample counts are before outlier removal.

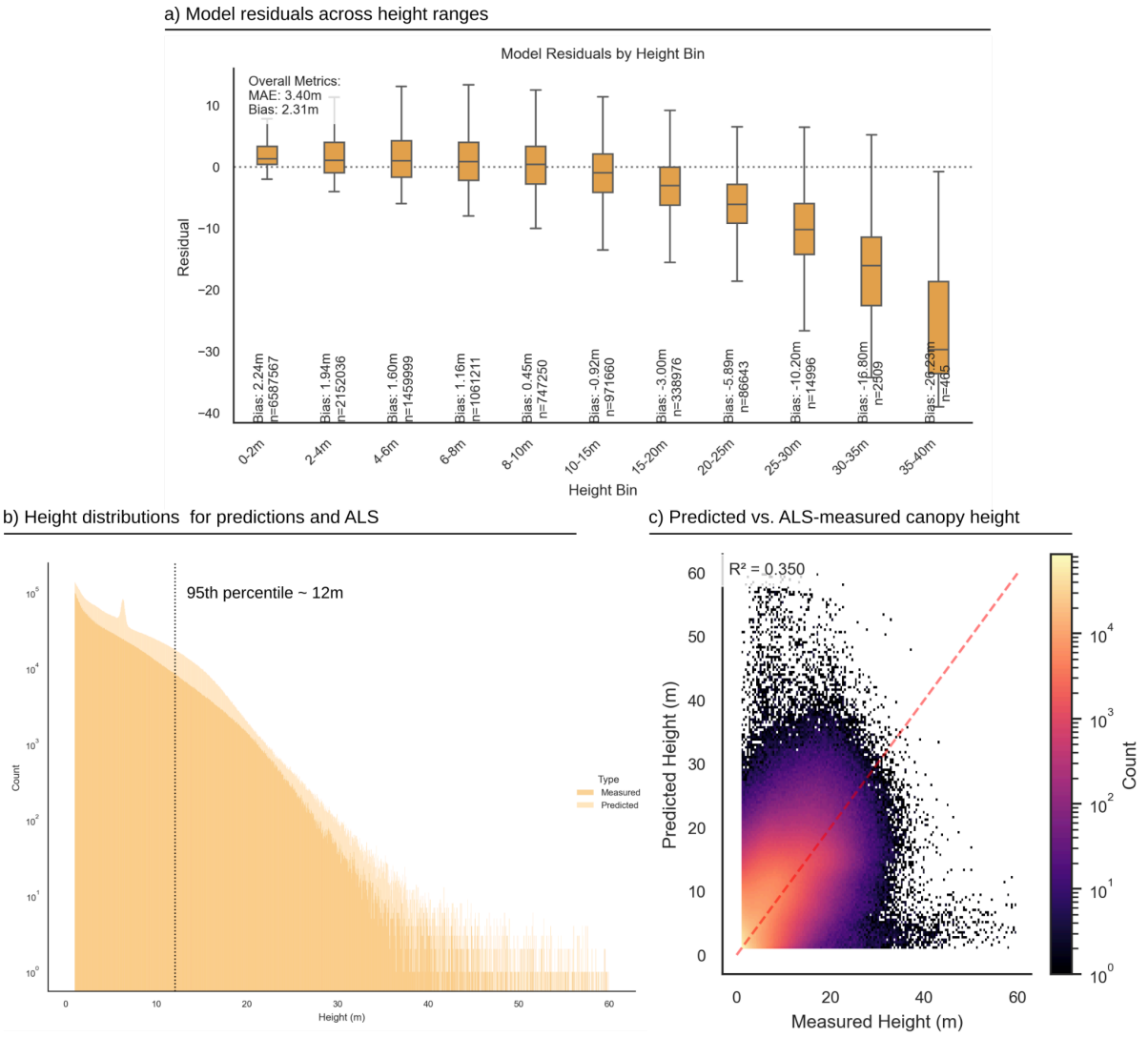

Figure S2. Validation of the canopy height DL model. a) Residuals across height ranges, specifying bias and number of samples for each range. b) Comparison of height distributions obtained from ALS measurements (darker orange) and model predictions (lighter orange). The dotted line depicts the 95th percentile of ALS measured heights. c) Model predictions against ALS heights, the colour shows the number of samples with lighter colors representing larger numbers.

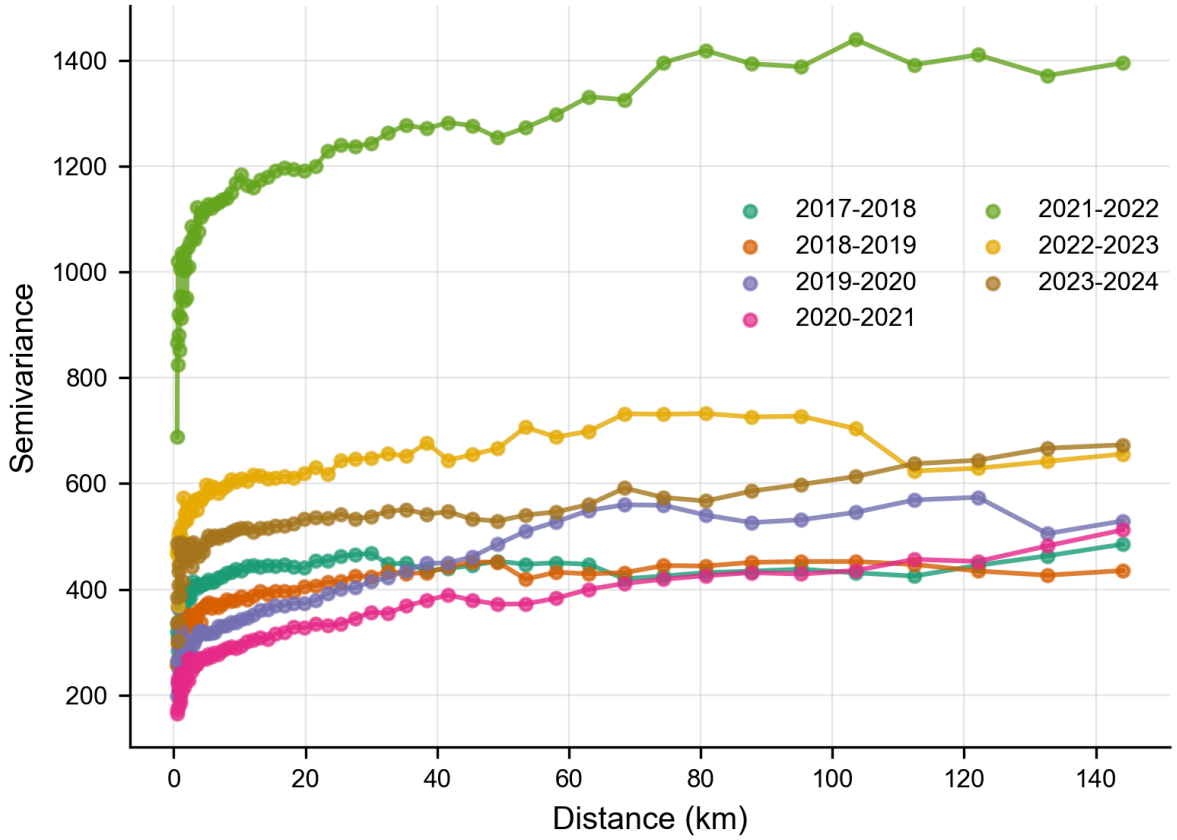

Figure S3. Variograms of relative interannual changes of carbon stocks for 2017-2024. Distance at semivariance saturation is a proxy of spatial autocorrelation distance in the data. We observe steep semivariance increases until 10 km, highlighting large autocorrelation at those scales, then increases become less pronounced, with curves saturating between 40-80 km.

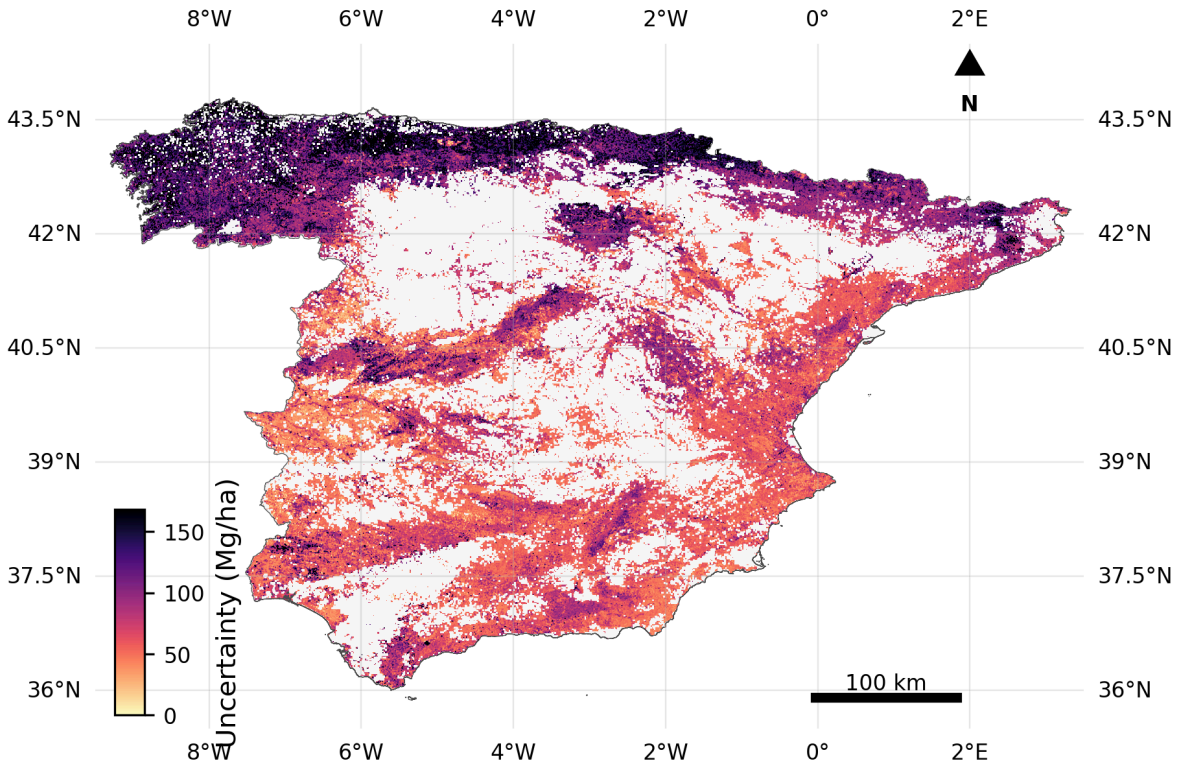

Figure S4. Uncertainty map of total carbon storage (belowground and aboveground) for 2024. The uncertainty level corresponds to 95% confidence intervals.

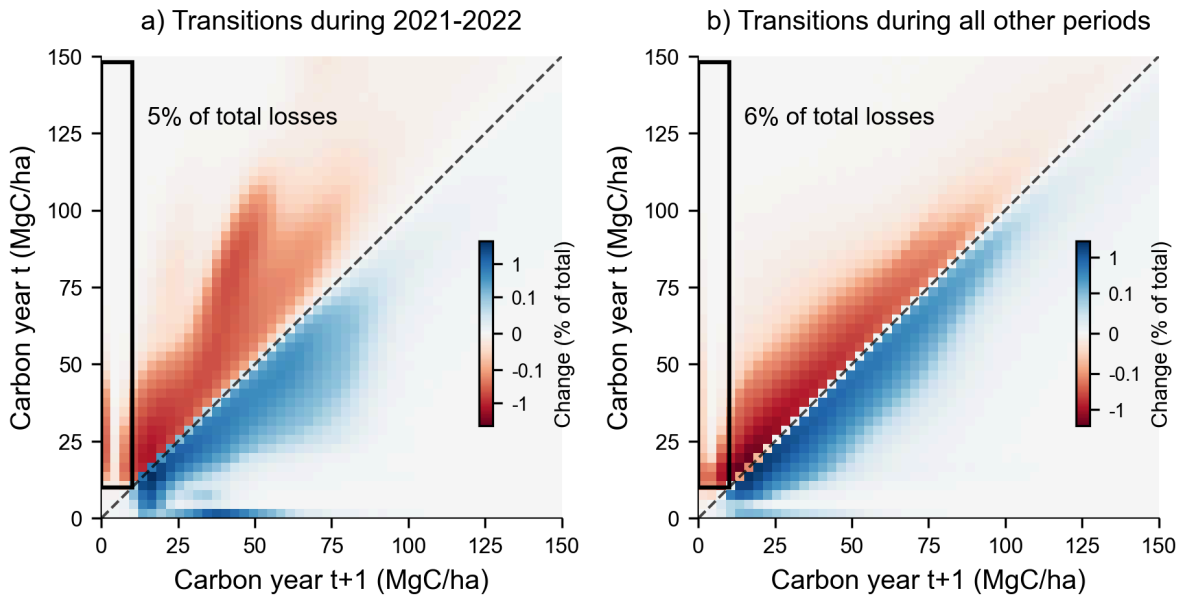

Figure S5. Pixel-level biomass carbon transitions between consecutive years for 2021-2022 (a) and all other periods combined (b). The y-axis represents initial carbon stocks and the x-axis represents final stocks, with colors indicating gains (blue) and losses (red). Pixels along the 1:1 line indicate no change. The black rectangle encompasses transitions from any initial biomass to <10 $MgC.ha^{-1}$, representing deforestation, timber extraction, or fire damage (5-6% of total losses). During most periods except 2021-2022, transitions cluster near the 1:1 line, reflecting minor canopy reflectance changes. In contrast, 2021-2022 shows substantial deviations from the 1:1 line, indicating severe canopy degradation. Importantly, most predicted losses represent forest degradation rather than complete biomass removal, as evidenced by the low contribution of transitions to near-zero carbon stocks. This suggests that observed losses reflect compromised canopy condition in trees with retained stem biomass. However, this retained biomass will remain lost without recovery, meaning the potential carbon emission is time-lagged but real—our model predicts losses before they fully materialize. Conversely, successful recovery would manifest as biomass growth patterns in subsequent years.

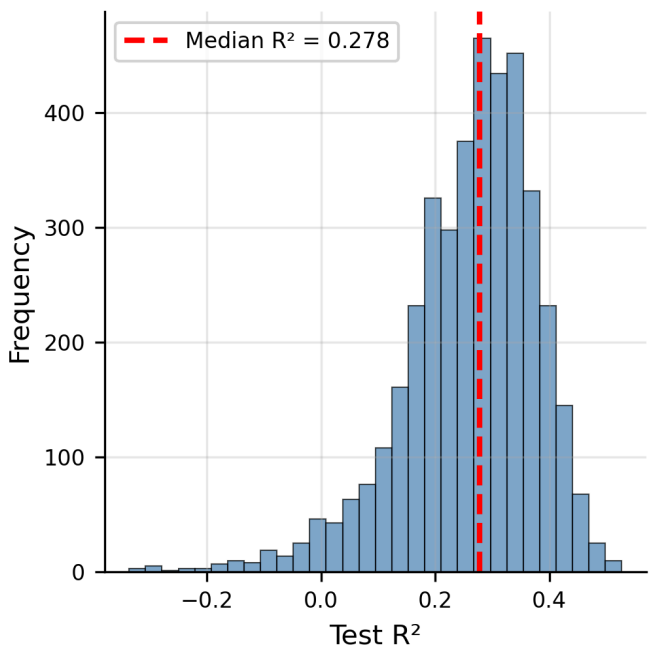

Figure S6. Distribution of goodness-of-fit (R2) of optimal models across 4,000 optimization experiments. The dotted red line depicts the median R2 across all experiments.

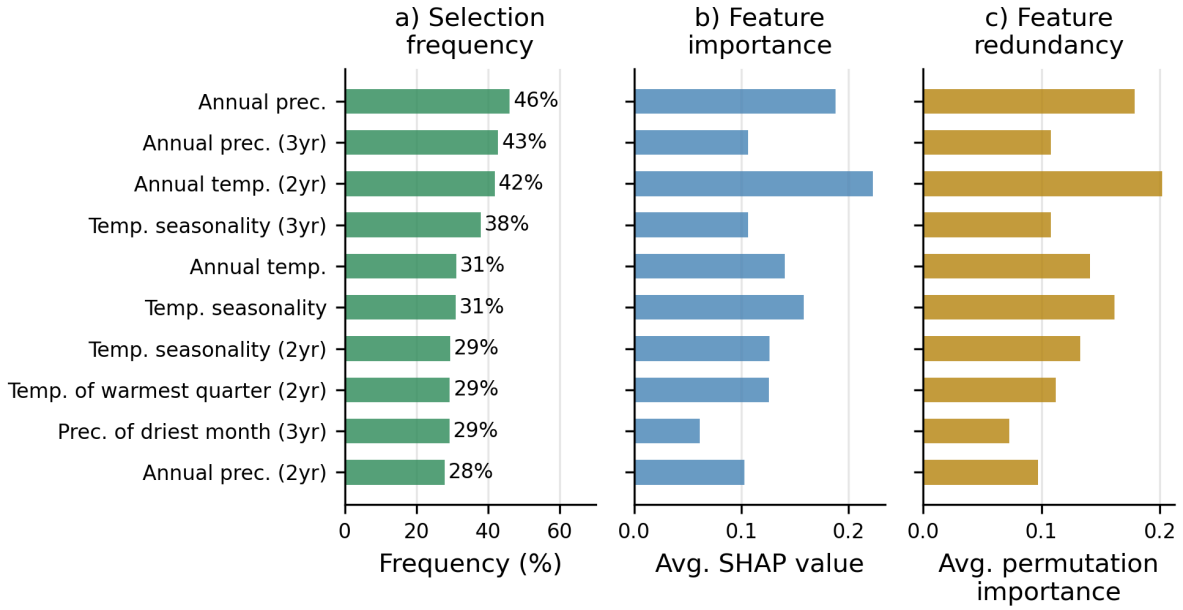

Figure S7. Most relevant bioclimatic anomalies for the prediction of interannual carbon changes in Spain over 2017-2024. The figure shows the 10 most frequently selected features across 4,000 optimization rounds. a) Percentage of optimal models including each feature. b) Average SHAP importance for each of the most selected features. c) Average permutation importance for each of the most selected features. Higher scores mean less redundancies. Notice the close agreement between feature ranking with respect to SHAP and permutation importances.

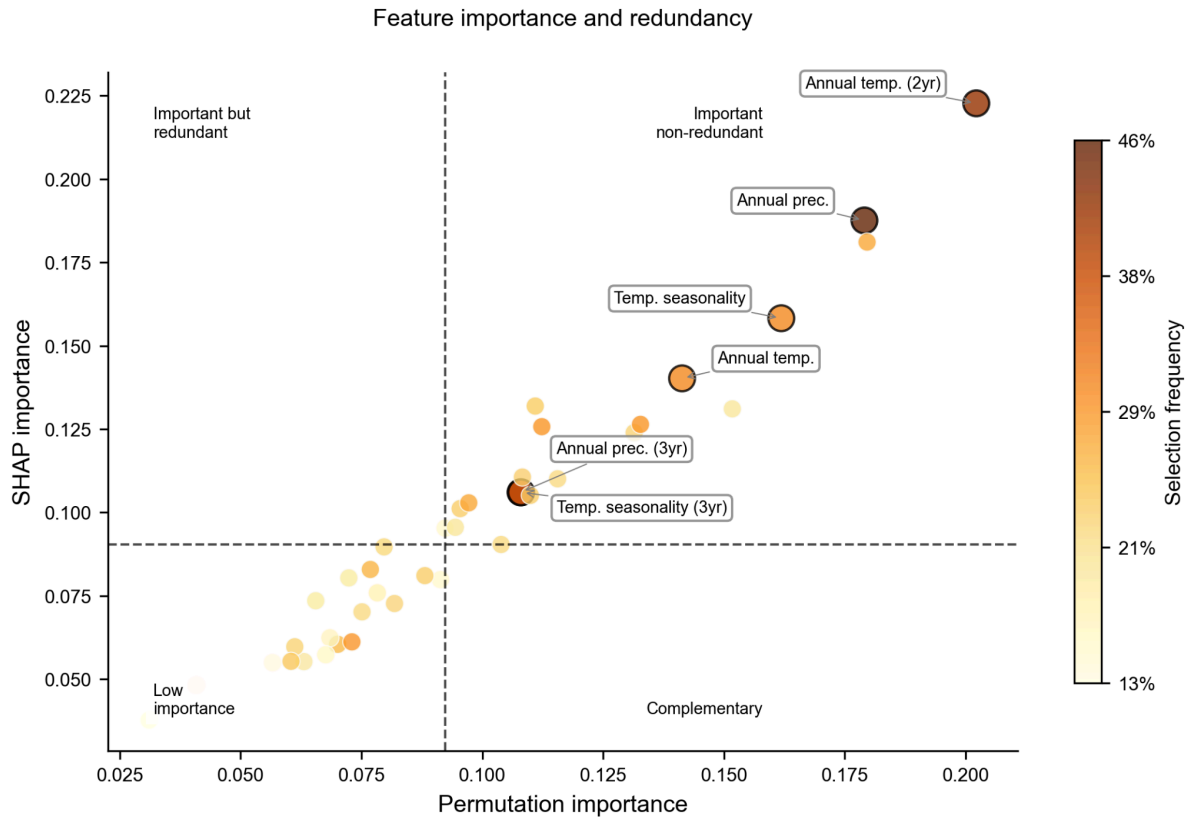

Figure S8. Feature importance (y-axis, measured by average Shapley values) versus redundancy (x-axis, measured by permutation importance) across 4,000 optimized XGBoost models. Colour represents the frequency of selection across all the optimized models with an R^2 larger than 0.2. Larger disks represent the six features most frequently selected, each appearing in at least 30% of models with $R^2 > 0.2$. Dotted black lines indicate median values of Shapley and permutation importance across all features. Most frequently selected features have also large SHAP importance and permutation importance values, supporting the robustness of our systematic procedure to identify the most relevant climatic drivers of interannual changes in woody carbon storage.

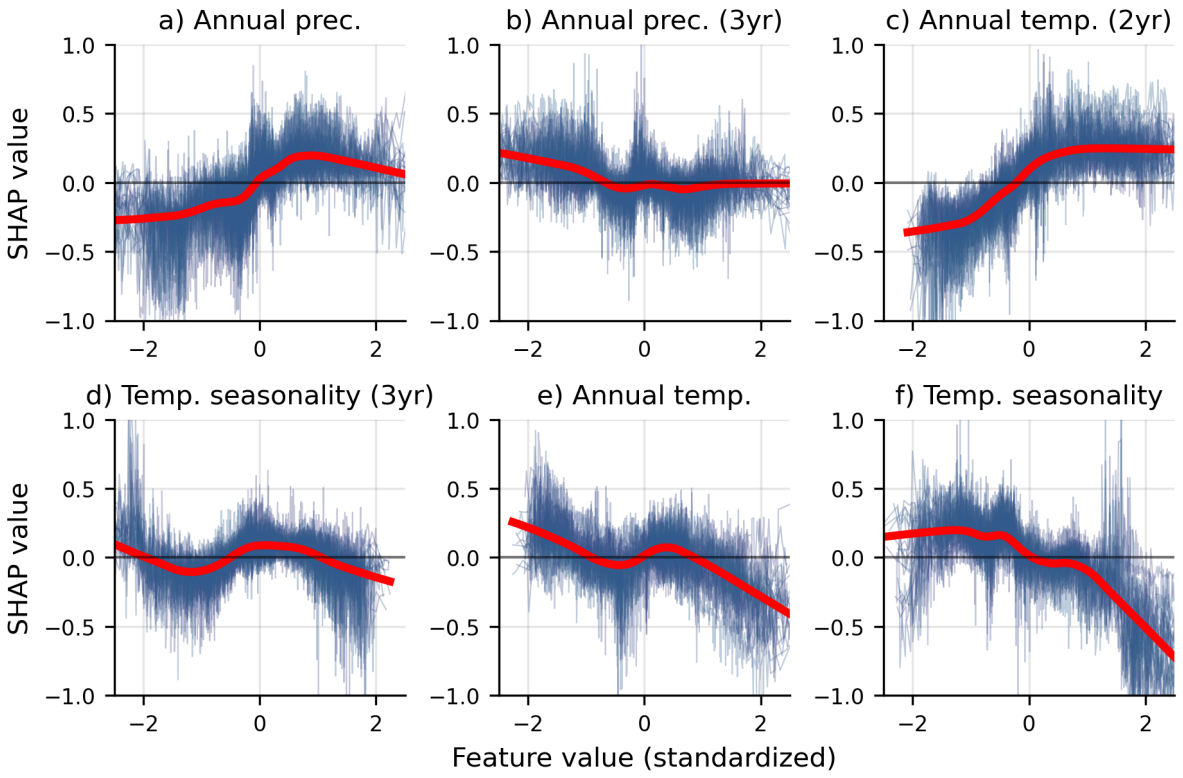

Figure S9. Partial dependence plots of SHAP and feature values for features selected in more than 30% of the optimal models. The plots show how SHAP values for each feature change with the feature value. Qualitative changes happen when SHAP values cross the horizontal 0 line, implying that effects change from positive to negative and vice versa. Positive SHAP values mean that feature values in that range lead to increases in the target variable, in this case interannual carbon changes. The larger the SHAP absolute value, the strongest the effect. Blue lines correspond to raw data (2,000 points) for each of the models including a feature and the solid red lines correspond to a LOWESS smoothing of the ensemble of models including each feature. Panels correspond to different variables.

Forest type	Dominant genus	Area (km^2)	Relative area (%)
Woodlands and agroforestry		**305,472**	**61.9**
Broadleaved		**105,404**	**21.3**
	Quercus	46,397	9.4
	Dehesas	28,376	5.7
	Mixed	17,046	3.5
	Eucalyptus	6,178	1.3
	Fagus	3,895	0.8
	Castanea	1,600	0.3
	Olea	895	0.2
	Betula	403	0.1
	Arbutus	274	0.1
	Fraxinus	144	0.0
	Corylus	86	0.0
	Ceratonia	72	0.0
	Ilex	37	0.0
	Arecaceae	1	0.0
Conifer		**68,944**	**14.0**
	Pinus	57,557	11.7
	Mixed	7,272	1.5
	Juniperus	3,981	0.8
	Abies	134	0.0
Mixed		**13,879**	**2.8**
Unclassified		12	0.0
Total		**493,710**	**100**

Table S1. Total area covered by different forest types and stratified by dominant genera according to national statistics published in the most up-to-date Spanish forest map (MFE25).

Forest type					Number of samples	Mean intercept	Mean slope	15th percentile intercept	15th percentile slope	85th percentile intercept	85th percentile slope	R^2	RMSE ($Mg.ha^{-1}$)
General					9604	3.32	0.56	2.70	0.51	4.04	0.46	0.44	47.9
	Broadleaved				3524	2.98	0.60	2.37	0.4	3.75	0.52	0.38	44.1
		Ericaceae			43	2.16	1.0	1.60	0.84	3.54	0.40	0.47	25.47
			Arbutus		43	2.16	1.0	1.60	0.84	3.54	0.40	0.47	25.47
				Arbutus unedo	43	2.16	1.0	1.60	0.84	3.54	0.40	0.47	25.47
		Fagaceae			2380	2.96	0.59	2.42	0.36	3.73	0.52	0.38	42.73
			Castanea		31	2.57	1.01	2.31	0.93	4.72	0.32	0.65	64.37
				Castanea sativa	31	2.57	1.01	2.31	0.93	4.72	0.32	0.65	64.37
			Quercus		2244	3.05	0.50	2.49	0.27	3.87	0.37	0.31	34.23
				Quercus faginea	380	3.36	0.36	2.78	0.16	4.13	0.21	0.19	31.74
				Quercus ilex	1218	3.12	0.31	2.52	0.0	4.12	0.1	0.13	26.5
				Quercus pyrenaica	559	2.79	0.68	2.38	0.45	4.06	0.39	0.35	51.21
		Mixed			675	3.02	0.58	2.35	0.49	3.80	0.453	0.40	47.1

			Native		553	3.02	0.59	2.43	0.45	3.78	0.51	0.38	41.5
				Atlantic	52	2.65	0.86	3.20	0.33	3.59	0.71	0.52	81.1
				Mediterranean	501	3.14	0.47	2.52	0.33	3.88	0.39	0.28	36.05
			Alien and native		14	1.85	0.91	1.71	0.43	2.65	0.83	0.48	56.05
		Oleaceae			11	3.49	0.42	3.73	0.07	5.1	0.0	0.11	74.34
			Fraxinus		10	3.49	0.42	3.73	0.07	4.16	0.34	0.31	34.95
		Riparian			369	3.80	0.49	3.54	0.25	4.43	0.56	0.26	150.54
	Conifer				4691	4.46	0.57	2.9	0.55	4.12	0.45	0.51	44.1
		Mixed			491	3.41	0.56	2.86	0.52	4.15	0.38	0.45	38.69
			Native		487	3.41	0.56	2.84	0.55	4.16	0.38	0.46	37.87
				Mediterranean	485	3.41	0.57	2.86	0.53	4.15	0.38	0.46	38.11
		Pinaceae			3950	3.48	0.56	2.93	0.59	4.15	0.44	0.50	45.45
			Pinus		3950	3.48	0.56	2.93	0.59	4.15	0.44	0.50	45.45
				Pinus halepensis	670	3.24	0.27	2.55	0.0	4.05	0.0	0.11	21.13
				Pinus nigra	821	3.75	0.52	3.26	0.44	4.57	0.31	0.39	51.42
				Pinus pinaster	1179	3.57	0.52	3.18	0.42	4.26	0.35	0.4	38.65
				Pinus pinea	218	3.66	0.32	3.38	0.07	4.34	0.15	0.23	28.35
				Pinus uncinata	10	2.18	1.04	2.36	0.91	4.30	0.27	0.85	20.41
	Mixed				1684	3.40	0.52	2.81	0.40	4.11	0.42	0.38	49.1

		Native			872	3.16	0.58	2.53	0.52	3.85	0.49	0.43	39
			Mediterranean		866	3.16	0.58	2.58	0.48	3.90	0.46	0.42	38.41

Table S2. Regression coefficients and performance metrics for height-biomass allometries. Linear regressions were performed in the logarithmic space to fit power-law allometries. R^2 is the regressions' coefficient of determination and RMSE the regression's root mean squared error. Slopes and intercepts reported for 15th and 85th percentiles correspond to the coefficients of quantile regression to establish uncertainty in biomass estimations through Monte Carlo sampling. The table is organized hierarchically, according to degree of specificity from the species to the clade, constrained by data availability. Forest type classification follows the Spanish official forest map (MFE25) . We discarded allometries with a number of samples lower than 10 or an R^2 smaller than 0.1, like with *Eucalyptus spp*. or *Pinus Sylvestris*.

Forest type					Number of samples	Mean ratio	5th percentile of ratio distribution	95th percentile of ratio distribution
General					23064	0.46	0.21	0.79
	Broadleaved				7719	0.6	0.23	0.81
		Betulaceae			26	0.48	0.26	0.7
		Dehesas			1533	0.45	0.32	0.67
		Ericaceae			82	0.63	0.28	0.8
			Arbutus		82	0.63	0.28	0.8
				Arbutus unedo	82	0.63	0.28	0.8

		Fagaceae			5717	0.54	0.22	0.8
			Castanea		116	0.6	0.2	1.33
				Castanea sativa	116	0.6	0.2	1.33
			Fagus		415	0.23	0.16	0.42
				Fagus sylvatica	415	0.23	0.16	0.42
			Quercus		5186	0.57	0.3	0.81
				Quercus faginea	565	0.47	0.41	0.56
				Quercus humilis	190	0.47	0.33	0.6
				Quercus ilex	2925	0.67	0.4	0.81

				Quercus petraea/Quercus robur	211	0.47	0.3	0.65
				Quercus pyrenaica	1096	0.44	0.27	0.67
				Quercus suber	317	0.36	0.25	0.52
		Mixed			1564	0.51	0.27	0.59
			Native		1237	0.52	0.27	0.79
				Alpine	69	0.47	0.28	0.73
				Atlantic	59	0.43	0.16	0.71
				Mediterranean	1109	0.52	0.28	0.8
			Alien and native		40	1.1	0.33	3.68

		Myrtaceae		258	2.41	0.38	6.2
			Eucalyptus	258	2.41	0.38	6.2
		Oleaceae		68	0.57	0.33	0.77
			Fraxinus	56	0.23	0.16	0.42
		Riparian		780	0.46	0.27	0.41
	Conifer			9922	0.36	0.2	0.57
		Cupressaceae		638	0.3	0.21	0.5
			Juniperus	638	0.3	0.21	0.5
			Juniperus spp.	60	0.41	0.25	0.63

				Juniperus thurifera	556	0.29	0.21	0.41
		Mixed			1019	0.34	0.2	0.58
			Native		967	0.35	0.22	0.58
				Alpine	55	0.45	0.24	0.66
				Mediterranean	909	0.34	0.22	0.56
		Pinaceae			8265	0.37	0.2	0.57
			Abies		43	0.25	0.16	0.48
				Abies alba	43	0.25	0.16	0.48
			Pinus		8222	0.37	0.2	0.57

				Pinus halepensis	1916	0.44	0.28	0.63
				Pinus nigra	1478	0.25	0.18	0.4
				Pinus pinaster	1818	0.29	0.22	0.38
				Pinus pinea	588	0.4	0.26	0.52
				Pinus radiata	74	0.09	0.02	0.34
				Pinus sylvestris	2117	0.43	0.28	0.63
				Pinus uncinata	231	0.57	0.37	0.73
		Other (production)			36	0.14	0.02	0.44
	Mixed				1976	0.45	0.26	0.7

		Native			1965	0.45	0.25	0.72
			Alpine		63	0.43	0.19	0.66
			Mediterranean		1895	0.45	0.26	0.73

Table S3. Mean and 5th and 95th percentiles of the belowground-aboveground biomass ratios distributions across forest types. The table follows the forest type classification from the official Spanish forest map (MFE25) and ratios are based on data reported in the fourth Spanish forest inventory (IFN4). Ratios were estimated hierarchically in function of the specificity level of inventory data using species-level data when available. Taxa with less than 25 samples was removed from the analysis.

Forest type					Number of samples	Skewness	Kurtosis	Normality
General					23064	0.57	-0.3	Normal
	Broadleaved				7719	0.21	-0.78	Normal
		Betulaceae			26	-0.1	-0.98	Normal
		Dehesas			1533	0.59	-0.08	Normal
		Ericaceae			82	-0.58	-0.56	Normal
			Arbutus		82	-0.58	-0.56	Normal
				Arbutus unedo	82	-0.58	-0.56	Normal
		Fagaceae			5717	-0.08	-0.97	Normal

			Castanea		443	0.91	-0.09	Normal
				Castanea sativa	443	0.91	-0.09	Normal
			Fagus		415	0.94	0.53	Normal
				Fagus sylvatica	415	0.94	0.53	Normal
			Quercus		5186	-0.03	-1.19	Normal
				Quercus faginea	565	0.50	0.62	Normal
				Quercus humilis	190	0.15	0.51	Normal
				Quercus ilex	2925	-0.88	-0.15	Normal
				Quercus petraea/Quercus robur	211	0.40	-0.38	Normal

				Quercus pyrenaica	1096	0.43	-0.21	Normal
				Quercus suber	317	0.42	-0.09	Normal
		Mixed			1564	0.28	-0.62	Normal
			Native		1237	0.52	0.27	Normal
				Alpine	69	-0.20	-0.42	Normal
				Atlantic	59	-0.15	-1.06	Normal
				Mediterranean	1109	0.12	-0.64	Normal
			Alien and native		40	1.35	1.19	Normal
		Myrtaceae			258	0.93	-0.08	Normal

			Eucalyptus		258	0.93	-0.08	Normal
		Oleaceae			68	-0.48	-0.46	Normal
			Fraxinus		56	-0.52	0.17	Normal
		Riparian			780	0.45	-0.65	Normal
	Conifer				9922	0.38	-0.15	Normal
		Cupressaceae			638	0.76	0.38	Normal
			Juniperus		638	0.76	0.38	Normal
				Juniperus spp.	60	0.72	-0.20	Normal
				Juniperus thurifera	556	0.54	-0.03	Normal

		Mixed			1019	0.61	-0.09	Normal
			Native		967	0.44	-0.34	Normal
				Alpine	55	0.17	-0.03	Normal
				Mediterranean	909	0.68	-0.11	Normal
		Pinaceae			8265	0.31	-0.26	Normal
			Abies		43	1.08	0.43	Normal
				Abies alba	43	1.08	0.43	Normal
			Pinus		8222	0.31	-0.26	Normal
				Pinus halepensis	1916	0.23	-0.26	Normal

				Pinus nigra	1478	0.74	0.21	Normal
				Pinus pinaster	1818	0.19	0.06	Normal
				Pinus pinea	588	0.04	-0.3	Normal
				Pinus radiata	74	0.91	-0.41	Normal
				Pinus sylvestris	2117	-0.21	-0.32	Normal
				Pinus uncinata	231	-0.05	-0.23	Normal
		Other (production)			36	1.15	-0.21	Normal
	Mixed				1976	0.62	-0.12	Normal
		Native			1965	0.63	-0.12	Normal

			Alpine		63	0.20	-0.42	Normal
			Mediterranean		1895	0.12	-0.64	Normal

Table S3. Kurtosis and skewness of the belowground-aboveground biomass ratio distributions across forest types used for normality testing.

Variable name (WorldClim)	Description
BIO1	Annual mean temperature
BIO4	Temperature seasonality
BIO5	Maximum temperature of warmest month
BIO6	Minimum temperature of coldest month
BIO7	Temperature annual range
BIO10	Mean temperature of warmest quarter
BIO11	Mean temperature of coldest quarter
BIO12	Annual precipitation
BIO13	Precipitation of wettest month
BIO14	Precipitation of driest month
BIO15	Precipitation seasonality
BIO16	Precipitation of wettest quarter
BIO17	Precipitation of driest quarter

Table S4. List of bioclimatic variables used as predictors of interannual carbon changes. We also used two-year and three-year accumulated variables for each bioclimatic variable, resulting in a total of 39 bioclimatic variables. Bioclimatic variables were calculated from the ERA5-Land dataset (Muñoz Sabater, 2019; Copernicus Climate Change Service (C3S), 2022) using the definition provided in WorldClim2 (Fick and Hijmans, 2017), both for the baseline 30-year period 1984-2014, as well as annually to estimate anomalies.